2013

Sulfur degassing at Erta Ale (Ethiopia) and Masaya (Nicaragua) volcanoes: Implications for degassing processes and oxygen fugacities of basaltic systems

J. M. de Moor

T. P. Fischer

See next page for additional authors

Citation/Publisher Attribution

de Moor, J. M., et al. (2013), Sulfur degassing at Erta Ale (Ethiopia) and Masaya (Nicaragua) volcanoes: Implications for the degassing processes and oxygen fugacities of basaltic systems, *Geochem. Geophys. Geosyst.*, 14, 4076–4108, doi:10.1002/ggge.20255
Available at: https://doi.org/10.1002/ggge.20255

Geochemistry Geophysics Geosystems G3

Article
Volume 14, Number 10
2 October 2013
doi: 10.1002/ggge.20255
ISSN: 1525-2027

Published by AGU and the Geochemical Society

Sulfur degassing at Erta Ale (Ethiopia) and Masaya (Nicaragua) volcanoes: Implications for degassing processes and oxygen fugacities of basaltic systems

J. M. de Moor
Department of Earth and Planetary Sciences, University of New Mexico, Albuquerque, New Mexico, 87131, USA (mdemoor@unm.edu)

Now at Observatorio Vulcanológico y Sismológico de Costa Rica, Universidad Nacional, Heredia, Costa Rica

T. P. Fischer and Z. D. Sharp
Department of Earth and Planetary Sciences, University of New Mexico, Albuquerque, New Mexico, USA

P. L. King
Institute of Meteoritics, University of New Mexico, Albuquerque, New Mexico, USA

Now at Research School of Earth Sciences, Australian National University, Acton, Canberra ACT, Australia

M. Wilke
Deutsches GeoForschungsZentrum, Helmholtzzentrum Potsdam, Potsdam, Germany

R. E. Botcharnikov
Institut für Mineralogie, Leibniz Universität, Hannover, Germany

E. Cottrell
National Museum of Natural History, Smithsonian Institution, Washington, D.C., USA

M. Zelenski
Institute of Experimental Mineralogy, Russian Academy of Sciences, Moscow, Russia

B. Marty
Centre de Recherches Petrographiques et Géochimiques, CNRS, Ecole Nationale Supérieure de Géologie, Vandoeuvre-les-Nancy,France

K. Klimm
Institut für Geowissenschaften, Goethe Universität Frankfurt, Frankfurt am Main, Germany

C. Rivard
European Synchrotron Radiation Facility, Grenoble, France

D. Ayalew
Department of Earth Sciences, School of Earth and Planetary Sciences, Addis Ababa University, Addis Ababa, Ethiopia

C. Ramirez
Red Sismológica Nacional, University of Costa Rica, San Jose, Costa Rica

K. A. Kelley
Graduate School of Oceanography, University of Rhode Island, Narragansett Bay Campus, Narragansett, Rhode Island, USA

[1] We investigate the relationship between sulfur and oxygen fugacity at Erta Ale and Masaya volcanoes. Oxygen fugacity was assessed utilizing $Fe^{3+}/\sum Fe$ and major element compositions measured in olivine-hosted melt inclusions and matrix glasses. Erta Ale melts have $Fe^{3+}/\sum Fe$ of 0.15–0.16, reflecting fO_2 of ΔQFM 0.0 ± 0.3, which is indistinguishable from fO_2 calculated from CO_2/CO ratios in high-temperature gases. Masaya is more oxidized at ΔQFM $+1.7 \pm 0.4$, typical of arc settings. Sulfur isotope compositions of gases and scoria at Erta Ale ($\delta^{34}S_{gas} - 0.5‰$; $\delta^{34}S_{scoria} + 0.9‰$) and Masaya ($\delta^{34}S_{gas} + 4.8‰$; $\delta^{34}S_{scoria} + 7.4‰$) reflect distinct sulfur sources, as well as isotopic fractionation during degassing (equilibrium and kinetic fractionation effects). Sulfur speciation in melts plays an important role in isotope fractionation during degassing and $S^{6+}/\sum S$ is <0.07 in Erta Ale melt inclusions compared to >0.67 in Masaya melt inclusions. No change is observed in $Fe^{3+}/\sum Fe$ or $S^{6+}/\sum S$ with extent of S degassing at Erta Ale, indicating negligible effect on fO_2, and further suggesting that H_2S is the dominant gas species exsolved from the S^{2-}-rich melt (i.e., no redistribution of electrons). High SO_2/H_2S observed in Erta Ale gas emissions is due to gas re-equilibration at low pressure and fixed fO_2. Sulfur budget considerations indicate that the majority of S injected into the systems is emitted as gas, which is therefore representative of the magmatic S isotope composition. The composition of the Masaya gas plume (+4.8‰) cannot be explained by fractionation effects but rather reflects recycling of high $\delta^{34}S$ oxidized sulfur through the subduction zone.

Components: 23,134 words, 11 figures, 6 tables.

Keywords: basalts; sulfur; oxygen fugacity; sulfur isotopes; gas chemistry.

Index Terms: 1043 Fluid and melt inclusion geochemistry: Geochemistry; 1041 Stable isotope geochemistry: Geochemistry; 1036 Magma chamber processes: Geochemistry; 1031 Subduction zone processes: Geochemistry; 4870 Stable isotopes: Oceanography: Biological and Chemical; 3613 Subduction zone processes: Mineralogy and Petrology; 3618 Magma chamber processes: Mineralogy and Petrology; 8413 Subduction zone processes: Volcanology.

Received 9 May 2013; **Revised** 12 August 2013; **Accepted** 15 August 2013; **Published** 2 October 2013.

de Moor, J. M., et al. (2013), Sulfur degassing at Erta Ale (Ethiopia) and Masaya (Nicaragua) volcanoes: Implications for the degassing processes and oxygen fugacities of basaltic systems, *Geochem. Geophys. Geosyst.*, *14*, 4076–4108, doi:10.1002/ggge.20255.

1. Introduction

[2] This study investigates sulfur (S) degassing processes and S sources through the study of S isotope compositions and speciation of magmatic gases and basaltic scoria from Erta Ale (Ethiopia) and Masaya (Nicaragua). The goal is to constrain conditions of degassing such as oxygen fugacity, temperature, and pressure in each system to ascertain primary magmatic S isotope compositions, assess S isotope fractionation, and investigate the relationship between S degassing and oxygen fugacity.

[3] The multiple valence states of S (2− to 6+) result in complex geochemical behavior in both low and high-temperature environments. Sulfur is one of the most abundant constituents of volcanic gases, occurring predominantly as SO_2 (S^{4+}) and H_2S (S^{2-}) and is an important volatile component of mafic magmas [*Giggenbach*, 1996]. Sulfur degassing has been proposed as a mechanism that modifies the oxygen fugacity of magmas [*Anderson and Wright*, 1972; *Burgisser and Scaillet*, 2007; *Kelley and Cottrell*, 2012] and subduction of oxidized sulfur (sulfate) may be partially responsible for oxidation of the subarc mantle [*Evans*, 2012; *Kelley and Cottrell*, 2009; *Klimm et al*., 2012]. Fluxes of SO_2 are routinely measured in volcano monitoring because atmospheric concentrations of this species are easily detectable due

to its absorption of ultraviolet light [*Galle et al.*, 2002; *Platt*, 1994; *Stoiber et al.*, 1983]. Sulfur dioxide is an important volcanic gas in terms of climate impact on earth due to the oxidation of SO_2 to sulfate aerosols in the atmosphere [*Sigurdsson*, 1990]. Volcanic degassing of S has also been proposed as an important source of surface sulfur on Mars [*Banin et al.*, 1997; *Settle*, 1979] and volcanic SO_2 has been proposed as an effective greenhouse gas in the martian climate [*Gaillard and Scaillet*, 2009] that may have allowed liquid surface water to exist [*Halevy et al.*, 2007; *Johnson et al.*, 2008]. On Earth, degassing of volcanic SO_2 during the Paleoproterozoic may have initiated the modern biogeochemical sulfur cycle and atmospheric oxygenation [*Gaillard et al.*, 2011]. The sulfur cycle is therefore important for chemical modification of Earth's reservoirs, and is intricately linked with planetary-scale redox conditions.

[4] Sulfur isotope compositions ($^{34}S/^{32}S$ reported in delta notation relative to the Canyon Diablo Troilite standard) provide a tool for studying the sulfur cycle, sources of sulfur, degassing processes, and magmatic redox conditions though distinguishing source compositions from fractionation processes can be problematic. Mid-ocean ridge basalts (MORB) have a $\delta^{34}S$ value of $+0.3 \pm 0.5$‰ [*Sakai et al.*, 1984] and variations in $\delta^{34}S$ of diamond-hosted sulfides suggest that the mantle may be heterogeneous due to subduction of material with variable S isotope composition [*Chaussidon et al.*, 1987]. In general, high $\delta^{34}S$ values are associated with more oxidized forms of S (sulfate) whereas relatively low $\delta^{34}S$ values are associated with reduced S such as in sulfides. High $\delta^{34}S$ values of arc lavas have been attributed to recycling of subducted sulfate through subduction zones [*Alt et al.*, 1993; *Mandeville et al.*, 1998; *Ueda and Sakai*, 1984]. Seawater sulfate has a high S isotope composition of +21‰ primarily due to the sequestration of pyrite with low $\delta^{34}S$ (typically ~40‰ lower than seawater sulfate) [e.g., *Kurtz et al.*, 2003] formed by microbial reduction of seawater sulfate in oceanic crust and delivery of sulfate with $\delta^{34}S \sim +11$‰ to the oceans from weathering of continental crust [e.g., *Holser et al.*, 1988]. Heavy S isotope signatures in magmas have also been used to argue for assimilation of oxidized crustal material [e.g., *Gurenko et al.*, 2001].

[5] Sulfur isotope fractionation in magmatic systems is controlled by sulfur valence state in gas and melt, crystallization of S-bearing minerals, degassing, and temperature (see *Marini et al.* [2011] for a review of fractionation processes). Hydrothermal processes are associated with complex isotopic fractionation due to multiple S valence states in vapors (H_2S, SO_2), fluids (SO_4^{2-}, S^{2-}, SO_3^{2-}, polythionates, S_3^-), and solid phases (sulfates such as anhydrite, elemental sulfur, pyrite, sulfides, and hauyne-nosean minerals), a wide range of temperatures, and slow isotopic equilibration at hydrothermal temperatures [e.g., *Delmelle et al.*, 2000; *Rye*, 2005]. Gas interaction with hydrothermal fluids and deposition or remobilization of hydrothermal minerals or sublimates can modify the isotope composition of fumarolic gases [*Delmelle et al.*, 2000; *Giggenbach*, 1987; *Menyailov et al.*, 1986; *Rowe*, 1994]. Whereas fumarolic gases are subject to modification of S isotope signature from magmatic values by hydrothermal processes, plume gases from open vent volcanoes are more representative of magmatic gas compositions [*Liotta et al.*, 2012]. Thus, in order to sample magmatic gases minimally affected by secondary processes this study focuses on the S isotope composition of persistent plumes directly emitted at high temperatures from open vent basaltic volcanoes. Sampling in close proximity to the degassing magma minimizes potential modification of gas S isotope compositions due to interactions with the atmosphere or hydrothermal systems.

[6] Equilibrium, mass-dependent S isotope fractionation is significant even at magmatic temperatures and is primarily a function of sulfur speciation in melts and gases [*Marini et al.*, 2011; *Sakai et al.*, 1982]. The more oxidized S species tend to be isotopically enriched in ^{34}S due to stronger covalent bonding with the heavy isotope. Precipitation of sulfide or sulfate mineral phases from S saturated melts may significantly alter the S isotope composition of the residual melt in systems with S dissolved in multiple valence states [e.g., *Marini et al.*, 2011]. Sulfur is dissolved in silicate melts as either S^{2-} or SO_4^{2-} (S^{6+}) in reduced and oxidized melts, respectively [e.g., *Jugo et al.*, 2010; *Wallace and Carmichael*, 1994; *Wilke et al.*, 2008], and is typically degassed as H_2S (S^{2-}) or SO_2 (S^{4+}) (although minor gas species may occur such as C-O-S species and metal-S species). Figure 1 schematically shows the isotopic fractionation between melt and gas for different degassing scenarios. A melt dominated by S^{2-} has lower $\delta^{34}S$ than SO_2 gas if isotopic equilibrium is attained. However, a melt dominated by SO_4^{2-} has higher $\delta^{34}S$ than SO_2 gas at equilibrium. Thus, equilibrium degassing of SO_2 can lead to evolution

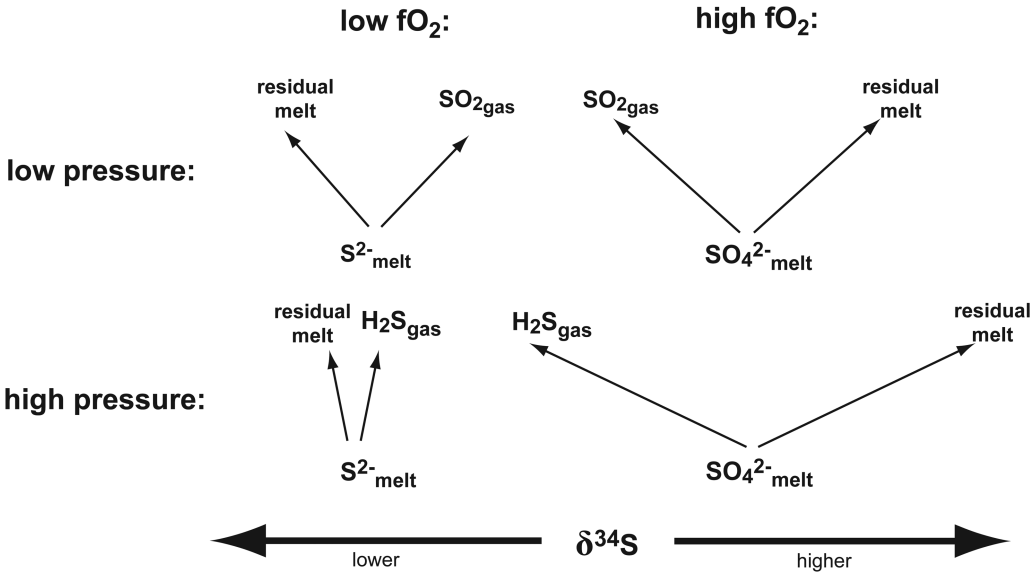

Figure 1. Schematic diagram showing end-member sulfur isotope fractionation degassing scenarios in simple melt-gas systems (i.e., no dense fluids or mineral phases). More oxidized S species bond more strongly with the heavy isotope, such that $\delta^{34}S$ $SO_4^{2-}>SO_2>H_2S\approx S^{2-}$. (top left) At equilibrium, if a melt containing S^{2-} degasses SO_2 gas, e.g., ΔQFM $\sim$0; P $\sim$1 bar) then the gas will have higher $\delta^{34}S$, resulting in residual melt with lower $\delta^{34}S$. (bottom left) The same melt degassing H_2S (e.g., P > 500 bars) will have little fractionation effect. Degassing of SO_2 or H_2S from a melt with dissolved SO_4^{2-} (high fO_2; e.g., ΔQFM $\sim$2) will result in residual melt with higher $\delta^{34}S$, but degassing of H_2S (P >> 500 bars) has a larger fractionation effect.

of a melt toward higher or lower $\delta^{34}S$ values depending on the dominant S species in the melt. A goal of this study is to evaluate isotopic equilibrium between magmatic gases and residual S in basaltic glasses from contrasting volcanic settings: a reduced rift zone and an oxidized subduction zone.

[7] Erta Ale and Masaya were chosen as representative end-members of basaltic sulfur degassing where plume gases can be sampled in close proximity to the magma source and where no previous reports of magmatic S-bearing minerals existed. Erta Ale is a relatively reduced system with oxygen fugacity (fO_2) close to the quartz-fayalite-magnetite (QFM) buffer [*Bizouard et al*., 1980; *Giggenbach and Le Guern*, 1976], whereas Masaya is relatively oxidized at ΔQFM >1 [*Mather et al*., 2006a]. Both volcanoes degas persistently from open vents and lack extensive hydrothermal systems. Here, we report S isotope compositions of plume gases and scoria from Erta Ale and Masaya, SO_2 gas fluxes, and constraints on fO_2, S speciation, and degassing temperature in order to assess S degassing, redox processes, isotope fractionation, and S sources in basaltic systems.

2. Geological Setting and SO_2 Fluxes

2.1. Erta Ale

[8] Erta Ale volcano (13.60°N; 40.67°E) is located in the Afar region of the East African Rift in northern Ethiopia (Figure 2a). Rifting and magmatism in this area are driven by the African Superplume, which is a tilted low-velocity mantle structure that extends from the core-mantle boundary below southern Africa to the base of the lithosphere below northern east Africa [*Ritsema et al*., 1999]. Helium isotope ratios in the region reach values as high as 15 R_A [*Pik et al*., 2006], where R_A refers to the He isotope composition relative to that of air, and olivines from Erta Ale have $^3He/^4He$ of 12.3 R_A [*Marty et al*., 1996], indicating primordial ^3He contribution from the lower mantle consistent with the influence of a deep plume. Radiogenic isotope and trace element compositions of basalts from the Erta Ale range are consistent with mixed depleted MORB and ocean island basalt (OIB) mantle sources [*Barrat et al*., 1998]. The crust in the region of Erta Ale was estimated by *Hammond et al*. [2011] to be 20 ± 2 km thick. Strontium and Nd isotopes indicate that no appreciable crustal contamination has influenced

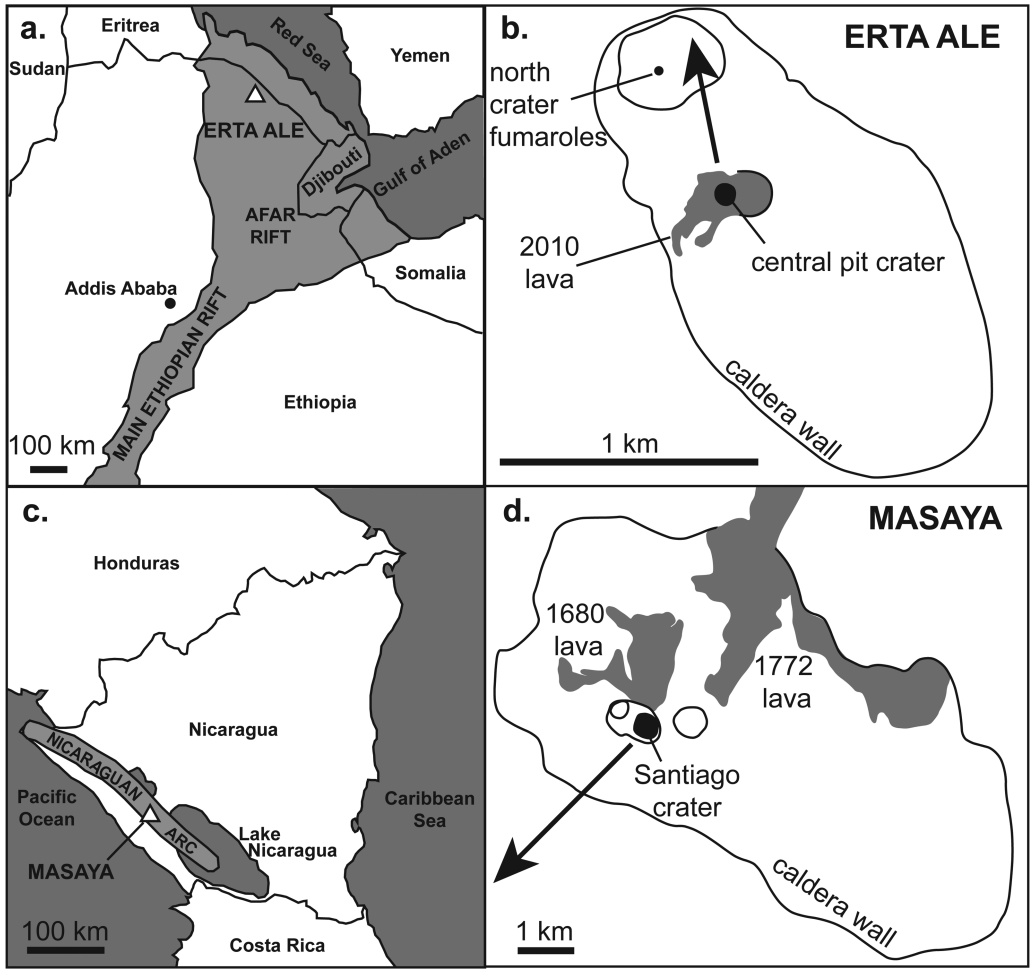

Figure 2. Schematic maps showing locations of (a) Erta Ale in the Afar triangle of the East African Rift, (b) the Erta Ale caldera, craters, and 2010 lava flow, (c) Masaya on the Nicaraguan segment of the Central American Arc, and (d) the Masaya caldera, craters, and lava flows erupted in 1680 and 1772. Bold arrows in Figures 2b and 2d show the dominant direction of the gas plumes at the time of sampling. Maps modified from *Field et al*. [2012], *Walker et al*. [1993], and *Williams* [1983].

these magmas and that the crust is young and basaltic [*Barberi and Varet*, 1970; *Barrat et al*., 1998]. Erta Ale has a low Ba/La ratio of 5.8 [*Zelenski et al*., 2013] between that of MORB (~4) and OIB (~10) [*Plank et al*., 2002]. The composition of Erta Ale basalts erupted in November 2010 are classified as transitional basalts and phenocrysts phases are plagioclase ($An_{83–74}$) + clinopyroxene ($En_{46–48}$, $Fs_{9–13}$, $Wo_{41–43}$) + olivine ($Fo_{84–78}$) with no oxides, sulfides, or accessory phases [*Field et al*., 2012]. The 2010 lavas (Figure 2b) are similar in composition to older erupted rocks [*Barberi and Varet*, 1970; *Barrat et al*., 1998; *Bizouard et al*., 1980; *Field et al*., 2012]. Sulfides and oxides only occur in the more evolved magmas in the Erta Ale suite (trachytes to peralkaline rhyolites) and crystallize as late phases [*Bizouard et al*., 1980].

[9] Degassing at Erta Ale takes place from two pit craters and a fumarole field located within the elliptical summit caldera (Figure 2b). The lava lake at Erta Ale has probably been active for over a century, and during the 1960's and 1970's both craters-hosted lava lakes [*Le Guern et al*., 1979; *Oppenheimer et al*., 2004; *Sawyer et al*., 2008]. Eruptions at Erta Ale are characterized by overflowing of the lava lake(s) and minor fire fountaining [*Le Guern et al*., 1979]. The latest eruption occurred in November 2010, just over 1 month before our expedition. Lava flows filled the central pit crater, overflowed into the main crater, and constructed a small spatter and cinder cone around the lava lake crater, which was about 15 m in diameter in January 2011.

[10] Sulfur dioxide flux measurements were conducted at Erta Ale in 2003 [*Oppenheimer et al*.,

Table 1. Sulfur Dioxide Fluxes From Erta Ale

Reference	Date	Source	Tons/d
This study	Jan 2011	Total	91.0
		Lava lake	60.2
Sawyer et al. [2008]	Oct 2005	Lava lake	59.6
Oppenheimer et al. [2004]	Mar 2003	Total	112.3
		Lava lake	60.5

2004], in 2005 [*Sawyer et al*., 2008], and in 2011 for this study. We conducted five walking traverses along the NW caldera wall in January 2011 using a thermally stabilized Ocean Optics UV spectrometer (see supporting information for details).[1] Errors on our measurements are estimated at ±30% and are reported in Table 1. In two out of the five traverses, the plume originating from the central crater lava lake was distinguishable from that emitted by the northern crater fumaroles. The average total SO_2 flux for Erta Ale in January 2011 was 91 tons/d (1σ of 24 tons/d), and the flux from the lava lake was ∼60.2 tons/d. Based on the available data (Table 1), the SO_2 flux from the lava lake appears to be constant, and has not changed since before the 2010 eruption. Similarly, the total SO_2 flux from the volcano in 2011 was within error of that in March 2003 (Table 1). Erta Ale is a minor contributor to the global volcanic SO_2 flux (36–77 ktons/d) [*Andres and Kasgnoc*, 1998; *Bluth et al*., 1993; *Graf et al*., 1997], with 100 tons/d representing just 0.1–0.3% of the global SO_2 flux. Considering the longevity of the lava lakes at Erta Ale, and the constant SO_2 flux, we consider the system to be close to steady state in terms of magma degassing rate.

2.2. Masaya

[11] Masaya (11.98°N; 86.16°W) is located in Nicaragua on the Central American Arc (Figure 2c), where the Cocos plate is subducted under the Caribbean plate at a rate of 77 mm/yr [*De Mets*., 2001]. Masaya is a tholeiitic basalt complex [*Martin and Sigmarsson*, 2007; *Walker*, 1989] that consists of nested calderas that have had several episodes of subsidence associated with Plinian explosive eruptions [*Williams*, 1983]. Phenocryst phases in erupted lavas are plagioclase, olivine, and clinopyroxene with magnetite as a minor phase [*Walker et al*., 1993]. The volcanoes of Nicaragua are characterized by the highest Ba/La [*Carr et al*., 1990] and ^{10}Be values [*Brown et al*., 1982] worldwide, indicating a strong slab component influence in magma genesis. Masaya has one of the highest Ba/La ratios (∼98) of the Central American volcanoes [*Carr et al*., 1990]. The crust beneath the Nicaraguan arc was estimated to be 25 ± 4 km thick by *MacKenzie et al*. [2008]. *Walker et al*. [1993] argued that major element, trace element, and $^{87}Sr/^{86}Sr$ compositions of post caldera lavas indicate little to no influence of crustal contamination, whereas the compositions older lavas suggest 15–30% assimilation of acidic igneous rocks.

[12] Recent activity is centered at Santiago crater (Figure 2d), which is ∼1 km in diameter and located at the summit of a young cone within the caldera. The volcano has been actively degassing for ∼150 years with episodes of intense gas emission "crises" with only minor magmatic ash eruptions [*Rymer et al*., 1998]. Sulfur dioxide flux measurements have been conducted since the 1970's [*Stoiber et al*., 1986] and there is a good temporal record for Masaya since the mid 1990's [*Martin et al*., 2010; *Nadeau and Williams-Jones*, 2009] (Figure 2). The average SO_2 flux since 1996 has been ∼1000 tons/d, representing 1.3–2.8% of global volcanic SO_2 emissions and ∼23% of the total SO_2 flux from Central American volcanoes [*Hilton et al*., 2002; *Mather et al*., 2006b]. Four traverses conducted on 11 January 2009 on the Llano Pacaya road for this study yielded a low SO_2 flux estimate of 325 tons/d (1σ of four traverses is 119 tons/d and these measurements are subject to large errors of ∼50%), indicating that at the time of sample collection Masaya was at a minimum in its degassing cycle (Figure 3). Causes of variability and sources of error in SO_2 flux measurements at Masaya are thoroughly discussed in *Nadeau and Williams-Jones* [2009] and *Martin et al*. [2010].

3. Methods

3.1. Gas Collection for Sulfur Isotope Composition and Complete Gas Chemistry

[13] We used a method for collection of plume S for isotopic analysis adapted from *Menyailov et al*. [1986]. Two bubblers were used in series and plume gas was pulled through the apparatus using a small electric pump at a flow rate of 1 L/m (Figure S1). The first bubbler contained 50 mL of 60 g/L zinc acetate (0.3 *M* $Zn(C_2H_3O_2)_2$) solution in 10% acetic acid, a method adapted from *Kiba et al*. [1955] for the collection of H_2S. The second bubbler contained 50 mL of 100 g/L barium chloride (0.4 *M* $BaCl_2.2(H_2O)$) in 10% H_2O_2 solution acidified to

[1]Additional Supporting Information may be found in the online version of this article.

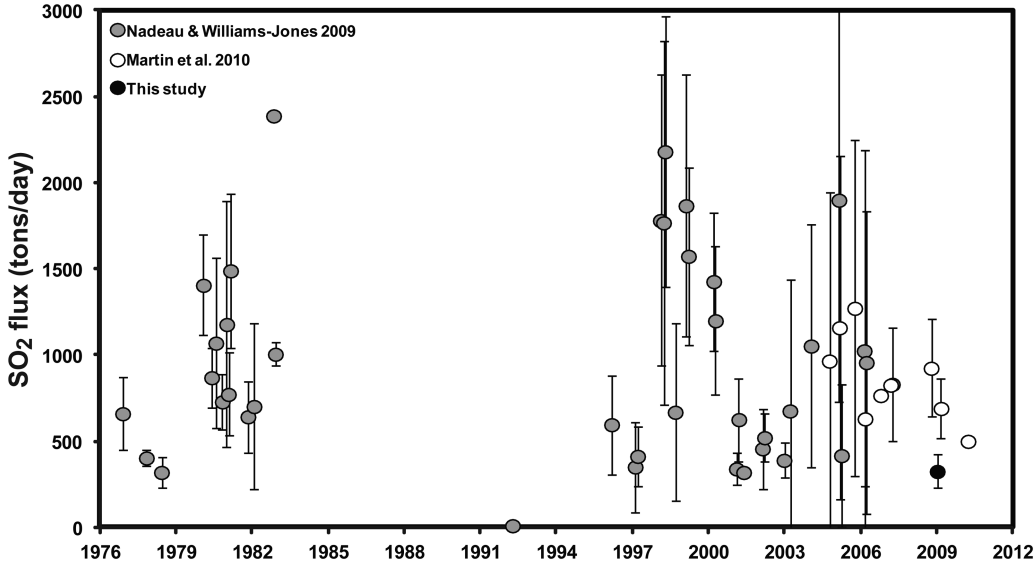

Figure 3. Sulfur dioxide flux record from Masaya. Data from compilations by *Nadeau and Williams-Jones* [2009] and *Martin et al*. [2010]. Also see references therein and data from *Martin* [2012].

pH 3 with HCl. Laboratory tests using pure, as well as diluted H_2S and SO_2, and gas mixtures, indicate that these solutions are highly efficient at stripping H_2S and SO_2 from the gas phase. Sulfur dioxide bubbled through two bubblers in series containing the $BaCl_2$ solution results in a precipitate in the first bubbler only, indicating that all SO_2 is stripped by the first. When used in series, H_2S is precipitated as ZnS in the first bubbler and SO_2 that is not dissolved in the first bubbler is precipitated as $BaSO_4$ in the second. The solution + ZnS from the first bubbler is centrifuged and the supernate is added to the solution from bubbler 2, which results in precipitation of dissolved SO_2 as $BaSO_4$. This solution is then centrifuged (with multiple rinses) and dried to collect pure $BaSO_4$. The ZnS from the first bubbler is converted to Ag_2S by addition of $AgNO_3$, centrifuged (with rinses) and dried. The $BaSO_4$ and Ag_2S are weighed to 10^{-3} mg precision to determine SO_2/H_2S ratio. Considering that ≤ 1 μg of ZnS precipitated from H_2S could go undetected and the average mass of $BaSO_4$ collected from SO_2 per sample was 85 μg the detection limit in terms of $H_2S/(SO_2 + H_2S)$ ratio is estimated to be ~0.05.

[14] The sample collection technique was tested to ensure that no isotopic fractionation occurred during sampling (Table S1, supporting information). Reference H_2S or SO_2 gas was bubbled through the sampling apparatus at a range of concentrations (pure or dilute H_2S, and 100% to <0.3% by volume SO_2) at flow rates up to 1 L/min. The resulting precipitates showed $\delta^{34}S$ values within analytical precision (1σ is <0.3‰) of the reference gas for both gases. The method was compared to the traditional Giggenbach method [*Giggenbach and Goguel*, 1989] at Sulfur Springs, NM, where bubbling hot springs emit H_2S and no SO_2 [*Goff et al*., 1985], and both methods gave identical results for $\delta^{34}S$ of H_2S (Table S1).

[15] Samples were collected from gas plumes at Erta Ale and Masaya as close as possible to the source. At Erta Ale, plume gas was collected ~30 m from the degassing lava lake surface and at Masaya gases were collected at the crater rim. A 1 μm pore size filter (47 mm diameter Polytetrafluoroethylene (PTFE)) was attached at the inlet of the sampling setup to collect plume sulfate aerosols. The apparatus was run until $BaSO_4$ precipitate was visible in the second bubbler and a typical sample resulted in the collection of 10–40 mg of $BaSO_4$ (0.05–0.2 mol S). No ZnS precipitate was observed in any of the plume samples from Erta Ale or Masaya. The filters from the inlet of the system were sonicated in 18 MΩ deionized water to dissolve sulfate aerosols, then precipitated as $BaSO_4$ by adding BaCl, centrifuged, dried, and weighed to determine SO_4^{2-}/SO_2 ratio.

[16] Gas samples were also collected from a high-temperature fumarole (1085°C) in the north crater of Erta Ale for complete gas chemistry and fO_2 assessment using techniques described by *Giggenbach and Goguel* [1989]. The fumarole was sampled using a quartz glass tube attached to silicon tubing and Giggenbach bottles containing ~50 mL of 4 *N* NaOH solution. Low solubility/inert gases partition into the headspace whereas

acid species dissolve in the NaOH solution. Headspace gases (N_2, O_2, H_2, He, Ar, and CO) were analyzed at the University of New Mexico on a Pfeiffer Quadrupole Mass Spectrometer (QMS; mass range from 0 to 120 amu) equipped with a Faraday detector and operated in dynamic mode. Calibration of the QMS was performed with standard gas mixtures (Scott Specialty Gases; Mix 14: 1% Ar, 1% He, 1% O_2, 1% CH_4, 1% CO, 95% N_2; Mix 104: 99.995% Ar, 0.005% N_2) and data processing using the Quadstar software that allows for correction of potential mass interferences. The QMS analyses have a precision of <0.1% (concentration). Carbon dioxide concentrations were determined by titration of NaOH solutions using 0.1 *N* HCl. Chloride and F concentrations were measured by ion chromatography on aliquots of caustic solution (i.e., 4 *N* NaOH solution + dissolved acid gases), diluted by a factor of ten, and filtered using Dionex OnGuard® II H cartridges to remove hydroxyl groups. Samples were analyzed on a Dionex ion chromatograph following the techniques of *Mitchell et al*. [2010]. Total S was determined gravimetrically after precipitation of $BaSO_4$ from the NaOH solutions, and SO_2/H_2S was measured by alkaline iodine titration [*Giggenbach and Goguel*, 1989].

[17] Argon isotope compositions were determined on splits of headspace gas at Centre de Recherches Pétrographiques et Géochimiques (CRPG), Nancy, France. Gas samples were transferred into high-vacuum metal containers, which were connected to the CRPG noble gas line held at 3×10^{-9} mbar. After overnight pumping, an aliquot of the gas was expanded into the line. It was purified sequentially over three getters working between 750°C and room temperature. Helium and neon were separated from other noble gases using a cryogenic trap (active charcoal at liquid nitrogen temperature) and analyzed (detailed method to be presented elsewhere). Argon was desorbed from the trap and analyzed with a noble gas static mass spectrometer (VG 5400). Blanks were always negligible (<1%) compared to the sample amounts. Uncertainties mostly represent the external reproducibility of the standard gas (atmospheric argon) which was relatively high during the analysis (though <5%) period because the mass spectrometer was settled for He isotope analysis and therefore had a low sensitivity for argon.

3.2. Scoria Sample Preparation

[18] Scoria from Erta Ale was collected from the cinder/spatter cone (N13°36.201′ E40°39.800′) formed during the November 2010 eruption. Scoria samples from Masaya were collected around the crater rim (N11°58.968′ W86°10.195′) and the freshest available scoria was picked in the field. In both cases, vesicular scoria consisted of clasts <2 cm. For isotopic analysis, unaltered scoria was picked from bulk samples and soaked in 18 MΩ deionized water for 24 h to remove any water-soluble sulfate on clast surfaces. Samples were then dried at 120°C and lightly crushed in a stainless steel mortar and pestle and sieved to <2 mm and >0.25 mm. This size fraction was then inspected under a binocular microscope and any visible crystals or altered fragments were removed, leaving 15–20 g of glass that was then rinsed in deionized water, dried, and pulverized in an Al_2O_3 ceramic shatterbox.

[19] Sulfur was extracted from the pulverized samples by reaction with "Kiba reagent" or tin (II) strong phosphoric acid, which is dehydrated phosphoric acid containing ~5% Sn^{2+}, following the methods of *Sasaki et al*. [1979]. The final product of the S extraction process is Ag_2S precipitate, which was separated from the solution by centrifuge with multiple rinses. The extraction method was tested for possible fractionation effects by converting sulfides, sulfates, and a basaltic glass with known $\delta^{34}S$ to Ag_2S. The samples used for these tests were an internal UNM lab pyrite sample ("Spanish pyrite"), barium sulfate precipitated from a 747°C gas sample (Giggenbach bottle method) from Momotombo volcano (Nicaragua) [*Elkins et al*., 2006], and a basaltic glass from the Juan de Fuca Ridge containing 1640 ppm S (P1326-2) (J. Stix and C. Mandeville, personal communication, 2009). No fractionation outside of analytical precision (~0.2‰) was observed: Spanish pyrite yielded +4.2‰ analyzed as FeS_2 and +4.0‰ analyzed as Ag_2S; Momotombo sample yielded +6.2‰ analyzed as $BaSO_4$ and +6.1‰ analyzed as Ag_2S. Silver sulfide derived from P1326-2 glass by Kiba extraction was analyzed twice, both analyses yielding $\delta^{34}S$ values of +1.4‰, which compare well with the value of $+1.7 \pm 0.65$‰ measured at University of Toronto on three replicate Kiba extractions of the same sample (B. Wing and J. Stix, personal communication, 2010)

[20] Olivine-hosted melt inclusions (Figure 4) and scoria samples were prepared for microanalysis to measure major elements, $Fe^{3+}/\sum Fe$, S concentration, and $S^{6+}/\sum S$. Olivines were separated from the lightly crushed scoria samples under binocular microscope and visually inspected for naturally

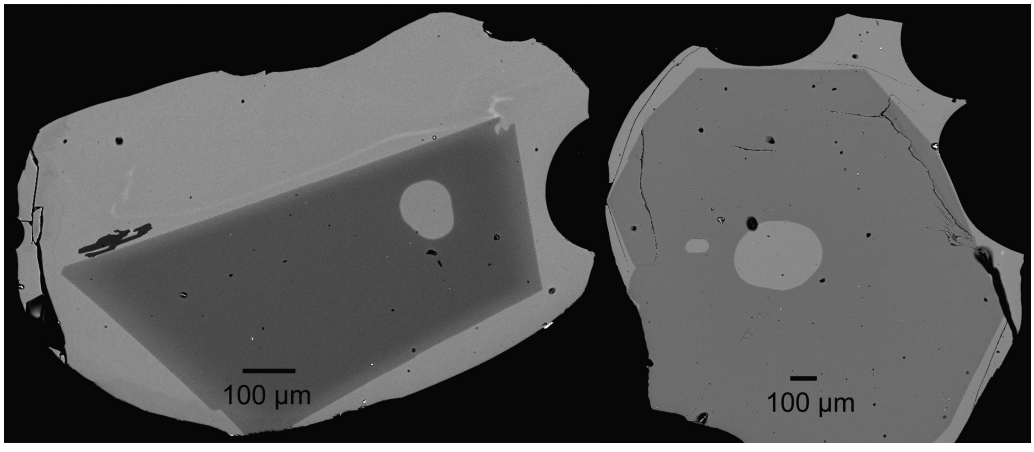

Figure 4. Back-scattered electron microscope images of olivine-hosted melt inclusions in glassy lapilli from Erta Ale 2010 eruption. The olivine is medium gray in color, surrounded by lighter glass and containing light gray melt inclusions.

glassy melt inclusions free of cracks. Olivines are relatively common in the Erta Ale samples, but exceedingly rare in the samples from Masaya. The melt inclusions were free of contraction vapor bubbles (except for one inclusion from Erta Ale) and showed smooth edges with no daughter crystals or rims of post entrapment olivine crystallization. Olivines were mounted in Epothin^{TM} epoxy, ground to expose the melt inclusions, and polished to 0.05 μm grit. Selected melt inclusions were mounted on quartzg lass disks and doubly polished for Fe and S X-ray absorption near-edge spectroscopy. Shards of matrix glass and scoria clasts were prepared in the same way as melt inclusions.

3.3. Sulfur Isotope Analysis

[21] Sulfur isotope measurements were conducted at the University of New Mexico by Continuous Flow Isotope Ratio Mass Spectrometry using a Costech Elemental Analyzer coupled to a Delta Plus XL Thermo Finnigan mass spectrometer via a Conflo II interface. Ag_2S or $BaSO_4$ (0.09–0.19 mg) is combusted in a quartz tube packed with ultrahigh purity copper wires and quartz chips at 1020°C in the presence of pure O_2 gas [*Fry et al.*, 2002]. By this method, the resulting SO_2 gas equilibrates with quartz chips at high temperature to fix the oxygen isotope composition of SO_2, which is then passed through a gas chromotograph (GC) column and measured in the mass spectrometer. International standards (all S isotope values are reported relative to the Vienna Canyon Diablo Troilite scale [*Robinson*, 1995] in $\delta^{34}S_{V\text{-}CDT}$ notation; IAEA-S-1 = −0.3‰ (Ag_2S), NBS123 = 17.44‰ (sphalerite), and NBS127 = 21.10‰ (barium sulfate) and a laboratory standard (CP1 = −4.60‰ (chalcopyrite)) were run at the beginning, at intervals between samples, and at the end of analytical sessions. Analytical precision calculated from the standards is better than ±0.3‰ (1σ). Analytical results were normalized to the standards listed above.

3.4. Electron Probe Microanalysis

[22] Electron probe microanalysis was conducted on a JEOL 8200 electron microprobe at the University of New Mexico. Glasses were analyzed (by wavelength dispersive X-ray analysis) for major elements and S, Cl, F using beam current of 10 nA, an accelerating voltage of 15 kV, and a beam diameter of 10 μm. Counting times were between 20 and 40 s for major elements, 60 s for S, and 40 s for Cl and F. Sulfur concentrations were measured using a spectrometer equipped with an LPET crystal with d-spacing of 4.375 Å and S k-α peak positions used in S concentration calibration were determined separately for Erta Ale and Masaya samples (∼5.37577 Å and ∼5.37221 Å, respectively). The detection limit for S was ∼ 20 ppm and secondary basalt glass standards (892-1, P1326-2, and JDF46N from Dr. Charles Mandeville and Dr. John Stix) were run to ensure accuracy. Precision is estimated at 5% relative for major elements and 10% relative for minor elements. Olivine phenocrysts were analyzed using a beam current of 20 nA, accelerating voltage of 15 kV and a beam diameter of 2 μm.

3.5. Iron and Sulfur Speciation Analysis by XANES

[23] Iron K-edge X-ray absorption near-edge structure (XANES) spectra were collected following the methods of *Cottrell et al.* [2009] on the X26A

beamline at the National Synchrotron Light Source at Brookhaven National Lab. Doubly polished wafers of glass and olivine-hosted melt inclusions were mounted on quartz glass slides. Spectra were collected in fluorescence using a Si (311) monochromator to control beam energy from 7020 to 7220 eV using a 9 × 5 μm X-ray spot. Sample location was confirmed using reflected light and Fe pre-edge peak mapping, though the large size of the melt inclusions (>100 μm for Erta Ale, Figure 4) ensured easy targeting of melt inclusions. Fluorescence yield was measured with 9 and 13 element Ge solid-state detectors. Basaltic standard glasses equilibrated at ΔQFM −2 to +4.5 (with $Fe^{3+}/\sum Fe$ 0.088–0.611) [*Cottrell et al*., 2009] were run twice during the 3 day analytical session, and a reference glass equilibrated at ΔQFM 0 (LW_0; $Fe^{3+}/\sum Fe$ 0.162) was run every few analyses to monitor and correct for drift. Three spectra were collected on each melt inclusion and spectra were carefully monitored for olivine interference, which is easily identified by the fine structure at the main edge and higher energies when crystals are in the beam path (see Figure S3 in supporting information). Between one and five spectra were collected on matrix glass samples depending on analyzable area. Spectra were deconvolved to quantify $Fe^{3+}/\sum Fe$ following the method of *Cottrell et al*. [2009]. The pre-edge energy interval from 7110 to 7118 eV was extracted from the raw spectra. A linear function and a damped harmonic oscillator function were used to subtract the baseline of the main Fe absorption edge. Two Gaussian curves were fitted to the pre-edge peaks and the area-weighted average of the Gaussian peaks (centroid) was used as the calibration parameter to calculate $Fe^{3+}/\sum Fe$. The centroid values were corrected for drift using the ΔQFM 0 reference glass (run every 2–5 analyses). Reproducibility of sample centroid values was ±0.01 eV. $Fe^{3+/}\sum Fe$ values were calculated from average centroid values following the calibration of *Cottrell et al*. [2009]. The precision of XANES using this suite of 13 standards is ± 0.005 in $Fe^{3+}/\sum Fe$ ratio of average centroid values (1σ values of average centroid values was 0.0036 for reference glass LW_0 for this analytical session), based on a full propagation of the uncertainty in each individual standard determined by Mössbauer spectroscopy ($Fe^{3+}/\sum Fe$ on a single standard by Mössbauer precise to ±0.02), as described by *Cottrell et al*. [2009]. The absolute accuracy is pinned to the accuracy with which $Fe^{3+}/\sum Fe$ ratios were determined on the standards by Mössbauer spectroscopy which, for these standards, agrees to within 1% with wet-chemical analyses [*Cottrell and Kelley*, 2011].

[24] XANES spectra at the S K-edge were collected at the European Synchrotron Radiation Facility (ESRF; Grenoble, France) at beamline ID21 using the scanning X-ray microscope (SXM). The setup uses a fixed-exit, Si (111) double-crystal monochromator to scan the energy of the incoming beam. The energy of the monochromator was calibrated using the position of the white line of the spectrum of gypsum (2482.84 eV). The incident beam intensity was measured using a photodiode and the spectra were collected in fluorescence mode using an energy dispersive Si-drift chamber solid-state detector with an active area of 80 mm^2. The beam was collimated using a pinhole to sizes ranging from 50 to 200 μm in diameter as required by the size of the melt inclusion. The energy was scanned quickly from 2450 to 2550 eV (400 steps) with a dwell time of 0.1 s per point. The quick-scans were stacked until an appropriate signal-to-noise ratio was achieved. The spectra were normalized by fitting the energy region before the edge with a polynomial function and subtracting it from the spectra to eliminate the background. The edge-jump was normalized to unity by fitting an arctangent and a Gaussian function to the spectra. For determining the sulfur oxidation state we used the method introduced by *Jugo et al*. [2010] and *Wilke et al*. [2011]. This method uses the signal intensity at specific energy positions of sulfide and sulfate. That is, the signal intensity for sulfide ($I(S^{2-})$) was integrated between 2475.7 and 2480 eV and the one for sulfate ($I(S^{6+})$), was integrated between 2481.5 and 2484 eV. The trend of $I(S^{6+})$ over the sum of the two signals ($\sum I = I(S^{2-}) + I(S^{6+})$) as a function of sulfur oxidation state was determined from a sequence of calculated spectra using the spectra of fully oxidized and fully reduced glasses where the energy position was calibrated using a gypsum standard. For this study we used the calibration by *Jugo et al*. [2010] for basaltic composition. The error is estimated to be ±0.02 in units of $S^{6+}/\sum S$.

4. Results

4.1. Sulfur Isotope Compositions of Gases and Scoria

[25] Sulfur isotope compositions of plume gas and scoria from Erta Ale and Masaya are reported in Table 2 and Figure 5a. No ZnS was precipitated

Table 2. Sulfur Isotope Compositions of Scoria and Plume Gas From Erta Ale and Masaya

Erta Ale		Masaya	
	$\delta^{34}S_{V\text{-}CDT}$‰		$\delta^{34}S_{V\text{-}CDT}$‰
Scoria		*Scoria*	
EA-R1	1.08	MAS-1a	7.80
EA-R2	1.11	MAS-1b	7.28
EA-R9	0.71	MAS-1c	7.91
EA-R10	0.51	*Mather et al.* [2006a]	6.60
Average	0.85	Average	7.40
1σ	0.29	1σ	0.60
Plume (SO_2)		*Plume (SO_2)*	
EA-BUB1-1	0.21	MSY1-1-2	5.13
EA-BUB1-2	−0.58	MSY1-2-2	4.25
EA-BUB1-3	−0.25	MSY1-3-2	4.49
EA-BUB1-4	−0.05	MSY2-2-1	5.06
EA-BUB1-5	−0.17	MSY2-3-1	5.35
EA-BUB1-6	−1.28	MSY2-4-1	4.72
EA-BUB1-7	−1.85	Average	4.83
EA-BUB1-8	−0.75	1σ	0.42
EA-BUB1-9	−0.32		
EA-BUB2-1	−0.07		
EA-BUB2-2	−0.70		
EA-BUB2-3	−0.62		
EA-BUB2-4	−0.35		
EA-BUB2-5	0.34		
EA-BUB2-6	−0.86		
EA-BUB2-8	−0.10		
EA-BUB2-9	−0.50		
EA-BUB3-1	−1.29		
EA-BUB3-2	0.21		
Average	−0.47		
1σ	0.57		

from plume gas at Erta Ale or Masaya, indicating that H_2S was an insignificant component of the gas (see section 3.1) and that S in these plumes is dominated by SO_2. Sulfate aerosol $\delta^{34}S$ values and SO_4^{2-}/SO_2 ratios are presented in Table 3. The SO_4^{2-}/SO_2 ratio measured in the Erta Ale plume was 0.006 ± 0.002 indicating that sulfate aerosols (average $\delta^{34}S$ value of $+1.9 \pm 0.5$‰) are an insignificant proportion of the total S in the plume. Sulfur isotope compositions of plume gas (SO_2) from Erta Ale has a value of -0.5 ± 0.6‰ with a range of −1.9‰ to +0.3‰, whereas scoria from Erta Ale have an average value of $+0.9 \pm 0.3$‰ with a range of +1.1‰ to +0.5‰. These values span the range for MORB ($+0.3 \pm 0.5$‰) [*Sakai et al.*, 1984], and the gas has a $\delta^{34}S$ composition about 1.3‰ lower than that of scoria.

[26] Plume gas (SO_2) from Masaya has a S isotope composition of $+4.8 \pm 0.4$‰ whereas scoria yield $\delta^{34}S + 7.4 \pm 0.6$‰ (Table 2). These values are significantly higher than MORB, and fall in the range of arc products from mafic volcanoes [*Alt et al.*, 1993; *de Hoog et al.*, 2001; *Menyailov et al.*, 1986; *Taran et al.*, 2002, 1995]. Similar to Erta Ale, the gas is isotopically lighter than the scoria, however, the difference between gas and scoria is

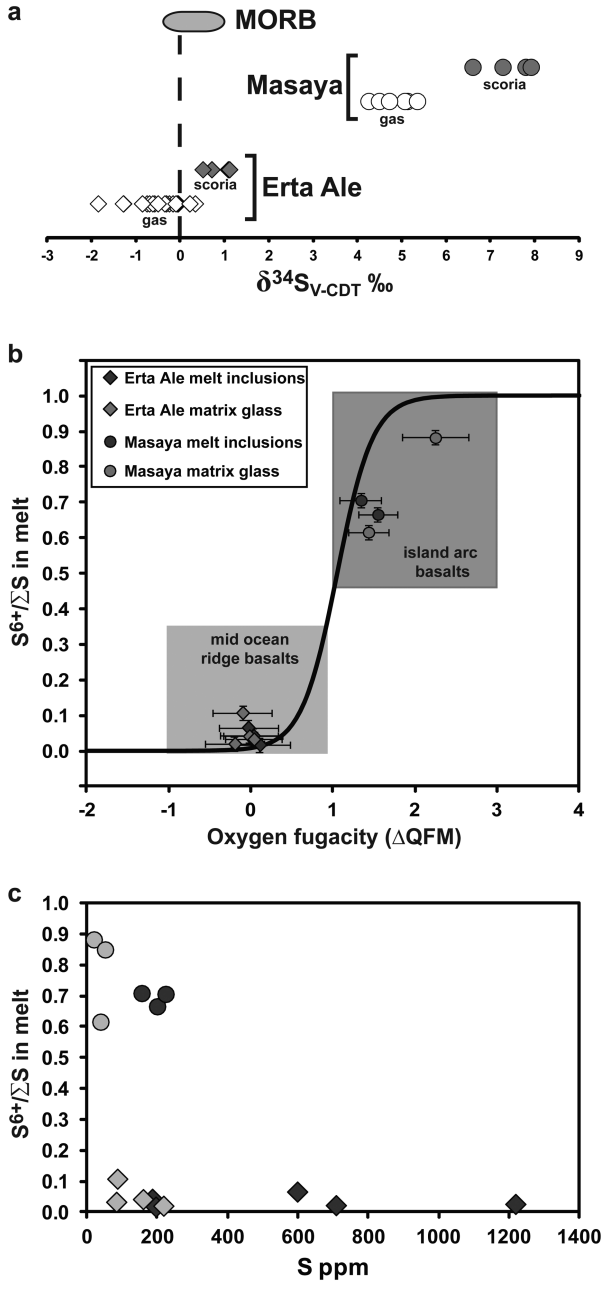

Figure 5. (a) Sulfur isotope compositions of plume gas (SO_2) and scoria from Erta Ale and Masaya as well as the field for MORB from *Sakai et al.* [1984]. Analytical uncertainty is ~0.2‰. (b) Sulfur speciation by S XANES versus oxygen fugacity calculated from $Fe^{3+}/\sum Fe$ and major element compositions of melt inclusions and matrix glass for Erta Ale and Masaya. The ranges for mid-ocean ridge basalts and island arc basalts are from *Jugo et al.* [2010], as is the experimentally determined relationship between $S^{6+}/\sum S$ and oxygen fugacity (black curve). (c) Sulfur speciation in the melt (melt inclusions and matrix glass) versus S concentration for Erta Ale and Masaya.

Table 3. Sulfur Isotope Compositions of Sulfate Aerosol, SO_4/SO_2 Molar Ratios and $\Delta^{34}S$ SO_4-SO_2 in the Erta Ale and Masaya Plumes

Sample ID	SO_4/SO_2	$\delta^{34}S$ V-CDT	$\Delta^{34}S$ SO_4-SO_2
ERTA ALE			
Low Flow Pump (1 L/min) in Series With Bubblers			
EA-BUB1-FILT1	0.005	1.33	1.50
EA-BUB1-FILT2	0.008	n.d.	n.d.
EA-BUB1-FILT3	0.006	1.66	2.19
EA-BUB2-FILT1	0.007	1.51	1.52
EA-BUB2-FILT2	0.001	n.d.	n.d.
EA-BUB3-FILT1	0.007	1.75	2.29
EA-FILT4	0.006	3.09	3.39
Average	0.006	1.87	1.87
1σ	0.002	0.70	0.43
High Flow Pump (18 L/min)			
EA-FILT1		1.40	
EA-FILT2a		2.19	
EA-FILT2b		2.17	
EA-FILT5		1.85	
Average		1.90	
1σ		0.32	
MASAYA			
Low Flow Pump (1 L/min) in Series With Bubblers			
MSY1	0.036	7.8	3.2
MSY2	0.023	7.0	1.9
High Flow Pumps, Filter Packs, Tube Diffusive Samplers			
Allen et al. [2002]	0.01		
Martin et al. [2010]	0.005		
Mather et al. [2006a, 2008]		7.7 ± 0.8	~2.6[a]

[a]*Mather et al.* [2008] showed that S isotope composition of SO_2 collected on $NaHCO_3$ impregnated filters increases with filter loading (i.e., the amount of S and Cl collected on the filter). Thus, their minimum estimate for the S isotope composition of SO_2 (+5.1‰) at Masaya is used.

larger, at ~2.6‰. Estimates of SO_4^{2-}/SO_2 in the plume vary from 0.036 (this study) to 0.005 [*Allen et al.*, 2002; *Martin et al.*, 2010] and sulfate aerosol have an isotope composition of ~+7‰ to +8‰ (this study and *Mather et al.* [2006a]).

4.2. Sulfur Content and Major Element Chemistry and of Melt Inclusions and Matrix Glass

[27] Major and minor element compositions of melt inclusions and matrix glasses are reported in the supporting information in Tables S2–S5. The sulfur concentrations of olivine-hosted melt inclusions from Erta Ale vary between 140 and 1218 ppm (average = 394 ppm), whereas matrix glasses vary between 26 and 218 ppm (average = 112 ppm). Our melt inclusions from Masaya have low S content, from 92 to 224 ppm. *Sadofsky et al.* [2008] report S concentrations for olivine-hosted melt inclusions from Masaya of 296 to 480 ppm, *Wehrmann et al.* [2011] report values of ~430ppm for two inclusions, whereas *Horrocks* [2001] found that the highest S content measured in plagioclase-hosted melt inclusions was 220 ppm. The average S concentration of matrix glass from Masaya is 34 ppm (range is <20–52 ppm).

[28] Major element compositions of melt inclusions, host olivines, matrix glass and olivine rims were analyzed to assess melt temperatures (by liquid and olivine-liquid thermometry) and to determine whether melt inclusions were modified by post entrapment processes [e.g., *Putirka*, 2008]. Erta Ale melt inclusions and matrix glass are slightly more mafic (SiO_2 ~ 49.7wt %; MgO ~ 6.5 wt %; Mg# = 0.55) than those from Masaya (SiO_2 ~ 51.4 wt %; MgO ~ 5.0 wt %; Mg# = 0.48). Olivine host crystals at Erta Ale have compositions of $Fo_{79–82}$ whereas Masaya olivines have compositions of $Fo_{74–75}$. Masaya glasses are richer in K_2O (1.4 wt %) and FeO_T (13.0 wt %) and poorer in TiO_2 (1.3 wt%) and CaO (9.3 wt%) compared to Erta Ale glasses (0.6 wt% K_2O; 11.3 wt% FeO_T; 2.4 wt% TiO_2; 11.4 wt % CaO). Compositional differences between melt inclusions and matrix glasses are small for both volcanoes with relative differences for non-volatile elements of <5%.

[29] Erta Ale glasses are significantly more F rich (~500 ppm) than Masaya (~200 ppm) and matrix glasses are slightly enriched in F relative to melt inclusions in both systems. Masaya glasses have higher chlorine content (~500 ppm) than Erta Ale glasses (~260 ppm Cl), and matrix glasses are slightly depleted in chlorine relative to melt inclusions.

4.3. Iron and Sulfur Speciation and Oxygen Fugacity Calculations

[30] $Fe^{3+}/\sum Fe$ ratios are presented in Table 4. Melt inclusions from Erta Ale give values from 0.157 to 0.162, overlapping with the range observed in matrix glass of 0.147–0.160. Melt inclusions from Masaya have higher $Fe^{3+}/\sum Fe$ ratios of 0.232–0.262 and matrix glasses are more oxidized with a range of 0.252–0.328. These values for the Masaya melt are in good agreement with the Mössbauer results from *Mather et al.* [2006a] which show $Fe^{3+}/\sum Fe$ values 0.23–0.31 in whole rock scoria. Measured $Fe^{3+}/\sum Fe$ values were used in assessing K_D for Fe^{2+}/Mg between melt inclusions and olivine host crystals in order to assess post entrapment modification (see section

Table 4. Results of $S^{6+}/\sum S$ and $Fe^{3+}/\sum Fe$ Measurements and fO_2 Calculations[a]

				1 bar					1.5 kbar				
	S (ppm)	$S^{6+}/\sum S$	$Fe^{3+}/\sum Fe$	T (°C)	log fO_2	±	ΔQFM	±	T (°C)	log fO_2	±	ΔQFM	±
Erta Ale													
Melt Inclusions													
EA-MI-4	598	0.067	0.157	1151	−8.92	0.96	−0.04	0.34	1160	−8.65	0.95	0.01	0.34
EA-MI-13_2	186	0.044	0.157	1155	−8.81	0.96	0.03	0.35	1163	−8.55	0.95	0.08	0.34
EA-MI-7	196	0.018	0.162	1156	−8.72	0.95	0.11	0.34	1165	−8.45	0.94	0.15	0.33
BS-H2-MI2	1218	0.027	n.a.	1161	n.a.		n.a.		1154	n.a.		n.a.	
EA-MI-1	708	0.023	n.a.	1152	n.a.		n.a.		1160	n.a.		n.a.	
Matrix Glass													
EA-R1	218	0.021	0.147	1149	−9.11	0.99	−0.20	0.36	1157	−8.85	0.97	−0.15	0.36
EAMI7_mg	160	0.043	0.156	1155	−8.86	0.96	−0.02	0.35	1163	−8.60	0.95	0.03	0.35
EAMI4_mg	87	0.108	0.151	1151	−8.99	0.97	−0.10	0.36	1159	−8.73	0.96	−0.06	0.35
EAMI13_mg	84	0.034	0.160	1148	−8.90	0.96	0.03	0.34	1156	−8.63	0.95	0.08	0.34
Masaya													
Melt Inclusions													
MAS-MI-2_1	200	0.666	0.262	1097	−8.03	0.91	1.54	0.24	1106	−7.76	0.23	1.59	0.23
MAS-MI-2_3	224	0.706	0.245	1099	−8.23	0.92	1.34	0.25	1107	−7.95	0.24	1.39	0.24
MAS-MI-3_1	156	0.709	n.a.	1120	n.a.		n.a.		1128	n.a.		n.a.	
Matrix Glass													
MAS1_cl1	48	n.a.	0.307	1127	−7.14	1.12	2.05	0.22	1127	−6.98	0.21	2.09	0.21
MAS1_cl2	20	0.883	0.328	1126	−6.96	1.11	2.24	0.21	1126	−6.80	0.20	2.29	0.20
MAS1_cl3	39	0.616	0.252	1127	−7.77	1.15	1.43	0.25	1127	−7.60	0.23	1.48	0.23

[a]Uncertainties in $S^{6+}/\sum S$ and $Fe^{3+}/\sum Fe$ ratios are ∼0.02. Oxygen fugacity was calculated based on the algorithm of *Kress and Carmichael* [1991] from $Fe^{3+}/\sum Fe$ ratios and major element compositions and ΔQFM values are relative to the quartz-fayalite-magnetite buffer of *Frost* [1991] at given P and T. Temperatures are calculated from the olivine-liquid geothermometer of *Putirka* [2008]. See text for details.

S2 in supporting information). No evidence is found for significant post entrapment effects.

[31] $S^{6+}/\sum S$ ratios of melt inclusions and matrix glass are reported in Table 4. Melt inclusions from Erta Ale yield $S^{6+}/\sum S$ ratios of 0.02–0.07 and matrix glasses display a similar range of 0.02–0.11. Glasses from Masaya are more oxidized, with melt inclusions showing $S^{6+}/\sum S$ ratios of 0.67–0.71 and matrix glasses displaying values of 0.62–0.88.

[32] Oxygen fugacities of the Erta Ale and Masaya melts are assessed for the temperature and pressure range relevant to S degassing and are reported relative to the QFM buffer of *Frost* [1991]. Temperatures used in the calculation of fO_2 (1156–1163°C for Erta Ale, 1097–1127°C for Masaya; errors are assigned as ±50°C following *Putirka* [2008]; Table 4) were based on the olivine-liquid geothermometer of *Putirka* [2008]. Temperatures derived from olivine-melt thermometry are in good agreement with the highest measured temperatures of the Erta Ale lava lake (1174°C) [*Oppenheimer et al*., 2004]. Oxygen fugacities were calculated from measured $Fe^{3+}/\sum Fe$ ratios and major element compositions for the range of pressure relevant to sulfur degassing from basaltic melts following the algorithm of *Kress and Carmichael* [1991]. *Lesne et al*. [2011] experimentally investigated the degassing behavior of S in basaltic melts with compositions based on Masaya and Stromboli and found that S partitions significantly into the gas phase at less than ∼1.5 kbar. Thus, oxygen fugacities were calculated for P = 1 bar and P = 1.5 kbar (Table 4) to bracket the P dependence of fO_2, and for temperatures derived from olivine-liquid thermometery. Uncertainties on the fO_2 values reflect the uncertainty in $Fe^{3+}/\sum Fe$ ratios (section 3.5) and temperature estimates (here taken to be ±50°C).

[33] The relationship between melt S speciation (measured by XANES) and melt fO_2 for Erta Ale and Masaya are shown in Figure 5b. Melt inclusions tend to show a better agreement with the curve of *Jugo et al*. [2010] than matrix glasses, perhaps because microanalyses of matrix glasses were not conducted on exactly the same spot whereas it is easier to target the same analytical area in melt inclusions. The relationship between S concentration and S speciation is shown in Figure 5c. No clear correlations between S concentration or S speciation is observed for either Erta Ale or Masaya

4.4. Oxygen Fugacity of Gases From Erta Ale

[34] Complete gas compositions for Erta Ale, as well as $^{40}Ar/^{36}Ar$ values, for gas samples collected in 2011 are reported in Table 5, together with a compilation of gas data available for Erta Ale. CO_2/CO ratios are used to calculate fO_2 in the gas phase by assessment of:

$$CO + 0.5O_2 \leftrightarrow CO_2 \quad (1)$$

following *Giggenbach* [1987] and using thermodynamic data from *Robie and Hemingway* [1995]. Whereas gas samples collected by *Giggenbach and Le Guern* [1976] and *Le Guern et al*. [1979] at Erta Ale in 1971, 1973, and 1974 show fO_2 values close to the QFM buffer, our samples show significantly higher CO_2/CO values, thus higher calculated fO_2 values. Importantly, our gas samples show Ar isotope compositions within analytical precision of the air value (295), and N_2/Ar and He/Ar ratios similar to air but O_2/Ar values lower than air (22.4). The fact that Ar isotope compositions are air like, whereas O_2/Ar is lower than air indicates that oxygen was consumed by combustion of reduced gas species upon mixing with air (within the sampled hornito) resulting in high CO_2/CO ratios.

[35] An overview of oxygen fugacities calculated from various sample types for Masaya and Erta Ale are shown in Figure 6.

5. Discussion

5.1. Oxygen Fugacity of Erta Ale and Masaya Magmas

[36] Oxygen fugacity is a parameter linked to the tectonic setting and differentiation history of melts. Melt inclusions and matrix glass from Erta Ale show indistinguishable fO_2 values in the range of ΔQFM -0.20 to $+0.15$, with uncertainty of <0.4 log units (section 4.3 and Table 4). These values are in remarkable agreement with fO_2 calculated from CO_2/CO ratios (22.0 ± 1.6; ΔQFM -0.2 ± 0.1) in high-temperature Erta Ale gas samples of *Giggenbach and Le Guern* [1976] as well as fO_2 for more evolved magmas from the Erta Ale suite from two-oxide thermobarometery [*Bizouard et al*., 1980]. In contrast, open path Fourier transform infrared (FTIR) measurements of gas emissions from Erta Ale yield higher CO_2/CO ratios of 57.1 ± 1.6 consistent with gas re-equilibration to measured gas temperatures [*Sawyer et al*., 2008] or high-temperature combustion of CO to CO_2. *Le Guern et al*. [1979] measured temperature increases with time on the surface of the lava lake, which they interpreted to reflect combustion of CO to CO_2 and H_2 to H_2O.

[37] Our own gas samples from a 1085°C fumarole show high and variable CO_2/CO ratios (56–89; Table 5) and significant mixing with air before discharging to the atmosphere, supportive of high-temperature combustion of CO to CO_2. The other reduced species that are susceptible to to oxidation by atmospheric O_2 are H_2 and H_2S. Equation (1) indicates that 1 mol of CO_2 produced by combustion consumes 0.5 mol of O_2. Oxidation of H_2 by:

$$H_2 + O.5O_2 \leftrightarrow H_2O \quad (2)$$

consumes 0.5 mol of O_2 for each mole of H_2 combusted. Oxidation of H_2S by [e.g., *Gerlach et al*., 1996]:

$$H_2S + 1.5O_2 \leftrightarrow SO_2 + H_2O \quad (3)$$

indicates that 1.5 mol of O_2 is consumed for each mole of H_2S converted to SO_2. Considering equations (1)–(3), the gas compositions can be restored to obtain the O_2/Ar ratio of air and the pre-air contamination values of CO_2/CO, H_2O/H_2, and SO_2/H_2S. Recalculation of our average gas composition (Table 5) to CO_2/CO, H_2O/H_2, and SO_2/H_2S to ΔQFM -0.1 at the maximum measured outlet temperature of 1085°C yields O_2/Ar of 22.5, that of air (22.4).

[38] These calculations indicate that combustion of CO, H_2, and H_2S by atmospheric O_2 is a significant process in modifying these gas compositions and that the pre-air contamination oxygen fugacity recorded by our gas samples is ΔQFM ~ -0.1. It is relevant to note that complete gas chemistry derived from direct sampling of gas emissions is the only available method for assessing the effects of atmospheric oxidation of reduced gas species in volcanic systems. For the case of Erta Ale, the fO_2 calculated from glass $Fe^{3+}/\sum Fe$ values and the restored gas compositions are in good agreement. The samples from *Giggenbach and Le Guern* [1976], the oxybarometry of *Bizouard et al*. [1980], and the results of this study all suggest that the gas and melt at Erta Ale have the same fO_2; i.e., that the gas is buffered by Fe in the melt, as proposed by *Giggenbach* [1987].

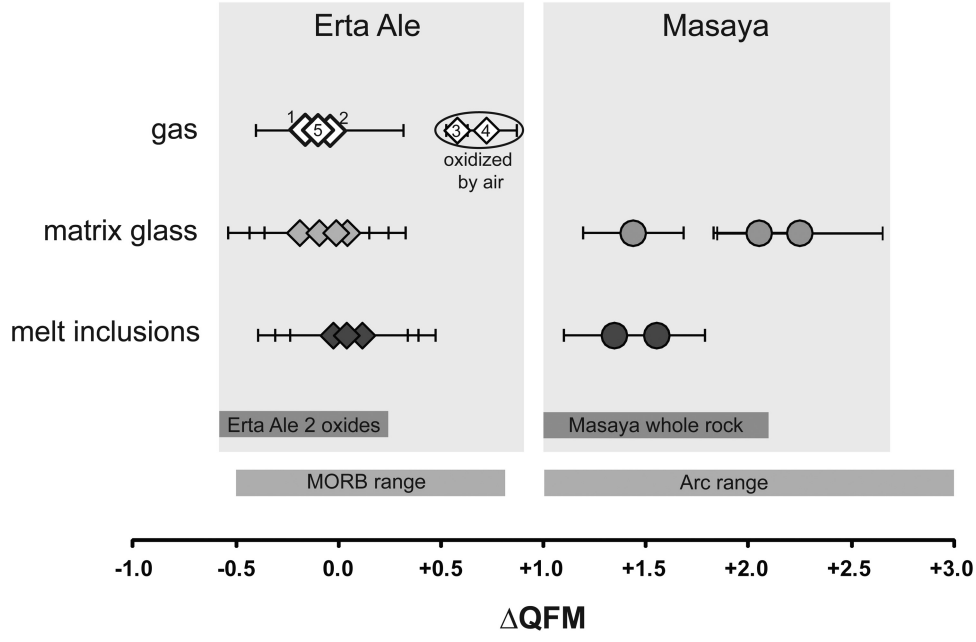

Figure 6. Comparison of oxygen fugacity estimates for different sample types for Erta Ale and Masaya. Melt inclusions and matrix glass from this study. MORB and Arc ranges from *Jugo et al*. [2010]. Erta Ale oxides ("Erta Ale oxides" field) from ilmenite and Ti-magnetite pairs from evolved rocks of the Erta Ale range series from *Bizouard et al*. [1980]. Oxygen fugacity estimates from CO_2/CO in gas phase: (1) *Giggenbach and Le Guern* [1976] samples collected in 1974, (2) *Le Guern et al*. [1979] samples collected in 1971, (3) *Sawyer et al*. [2008] plume measurements by FTIR, (4) Gas samples collected in 2011 for this study with fO_2 calculated from measured CO_2/CO, and (5) average for gas samples collected in 2011 corrected for atmospheric oxidation. Masaya whole rock field from Mössbauer measurements of Masaya whole rock [*Mather et al*., 2008], melt inclusions and matrix glass from this study. There are no fO_2 estimates available for gas emissions from Masaya.

[39] Masaya melt inclusions yield more oxidized fO_2 values of ΔQFM +1.3 to +1.6. One clast from Masaya shows matrix glass fO_2 (+1.48) in agreement with the melt inclusions, whereas two other clasts yield slightly higher fO_2 values of +2.09 and +2.29. Our $Fe^{3+}/\sum Fe$ ratios and fO_2 results are in agreement with those of *Mather et al*. [2006a]. The observation that Masaya glasses from the Central American Arc are significantly more oxidized than Erta Ale glasses from the East African Rift is consistent with prior studies showing that subduction zone magmas are more oxidized than magmas produced at spreading centers [e.g., *Kelley and Cottrell*, 2009].

5.2. Assessment of Possible Melt Saturation With Sulfide or Sulfate Mineral Phases and Degassing Prior to Melt Inclusion Entrapment

[40] No sulfide or sulfate minerals have been observed in our scoria samples from Erta Ale or Masaya, neither as an accessory phase nor as inclusions within phenocrysts. To our knowledge, there are no published reports describing S-bearing mineral phases in either system. Sulfides only occur in the more evolved magmas in the Erta Ale suite (trachytes to peralkaline rhyolites) and crystallize as late phases [*Bizouard et al*., 1980], and *Field et al*. [2012] found no oxides or sulfides in the 2010 lavas, consistent with this study and that of *Bizouard et al*. [1980]. Similarly, we have not found any S-bearing mineral phases in samples from Masaya, and oxides are the only accessory phase to occur in erupted products [*Martin and Sigmarsson*, 2007; *Walker et al*., 1993]. However, sulfide resorbtion may occur in basaltic systems [*Nadeau et al*., 2010; *Sisson*, 2003] and sulfide precipitation is a mechanism that could affect the S isotope compositions of magmas [e.g., *Marini et al*., 2011]. Therefore, in this section we address S solubility with respect to mineral phases.

[41] The melt sulfur content at sulfide or sulfate saturation (SCSS) is a function of melt composition, fO_2, fS_2, T, P, and H_2O content (see reviews

Table 5. Gas Compositions From Erta Ale, With Oxygen Fugacity Calculated Relative to the Quartz-Fayalite-Magnetite Buffer of *Frost* [1991][a]

Sample ID/ Reference	Year	Method	T (°C)	H_2O	CO_2	S_T	SO_2	H_2S	HCl	HF	He	H_2	Ar	O_2	N_2	CO	CO_2/CO	ΔQFM	O_2/Ar	$^{40}Ar/^{36}Ar$	±
EA-G-1	2011	Direct	1085	602.7	203.4	114.46	110.3	4.20	16.3	19.7	0.002701	7.368	0.3907	1.34	31.58	2.839	71.64	+0.73	3.4	292.2	10.7
EA-G-2	2011	Direct	1085	578.8	223.8	115.61	110.7	4.94	15.6	20.4	0.001654	7.499	0.4368	1.049	33.92	2.887	77.51	+0.80	2.4	293.8	10.4
EA-G-3	2011	Direct	1085	614.5	196.7	113.38	110.2	3.14	12.4	18.1	0.000343	4.886	0.4164	1.033	35.54	2.946	66.78	+0.67	2.5	295.5	10.9
EA-G-4	2011	Direct	1085	643	180.8	101.85	93.25	8.60	12.6	21.3	0.002462	6.521	0.3965	0.997	29.28	3.22	56.16	+0.52	2.5	289.9	10.7
EA-G-8	2011	Direct	1085	718.4	122.1	79.97	78.66	1.31	14.3	20.2	0.001336	2.701	0.4777	3.442	37.04	1.369	89.18	+0.92	7.2	n.a.	n.a.
Average	2011	Direct	1085	631.5	185.4	105.05	100.6	4.44	14.2	19.9	0.001699	5.795	0.4236	1.572	33.47	2.652	69.89	+0.71	3.7	292.9	
Average	2011	Recalc	1085	624.9	181.4	105.05	98.85	6.21	14.2	19.9	0.001699	12.375	0.4236	9.515	33.47	6.645	27.30	−0.11	22.5		
Sawyer et al. [2008]	2005	FTIR	730–1130	935.8	36.6	n.a.	24.7	n.a.	1.9	0.4	n.a.	n.a.	n.a.	n.a.	n.a.	0.6	61.00	−0.61 to +0.57	n.a.	n.a.	
Giggenbach and Le Guern [1976]	1974	Direct	1125–1135	794.0	104.0	73.6	65.0	8.6	4.2	n.a.	n.a.	14.9	0.01	0.5	1.8	4.6	22.61	−0.17	48.2	n.a.	
Le Guern et al. [1979]	1973	Direct	1100–1210	n.a.	547.3	n.a.	212.2	n.a.	n.a.	n.a.	n.a.	41.0	7.90	104.8	207.4	24.0	22.81	−0.17	13.3	n.a.	
	1971	Direct	1075	n.a.	365.2	220.9	219.5	0.5	n.a.	n.a.	n.a.	28.5	3.70	60.6	305.8	13.8	26.46	−0.05	16.4	n.a.	
Gerlach [1980]	1974	Recalc	1125–1135	771.3	117.0	88.9	73.0	9.2	n.a.	n.a.	n.a.	15.9	n.a.	n.a.	n.a.	5.2	22.50	−0.17	n.a.	n.a.	
	1971	Recalc	1075	695.6	178.0	99.4	87.9	9.5	n.a.	n.a.	n.a.	15.7	n.a.	n.a.	n.a.	7.8	22.82	−0.28	n.a.	n.a.	

[a]The O_2/Ar value for air is 22.4 and the $^{40}Ar/^{39}Ar$ value of air is 298.

by *Baker and Moretti* [2011] and *Backnaes and Deubener* [2011]). The *Liu et al*. [2007] solubility model is generally accepted as being successful in predicting SCSS [*Baker and Moretti*, 2011] except for the case of melts with high H_2O-contents, in which case SCSS is significantly underestimated [*Beermann et al*., 2012; *Moune et al*., 2009]. Olivine-hosted melt inclusions from Erta Ale have at most 0.15 wt % water [*Field et al*., 2012] indicating that it is appropriate to apply the *Liu et al*. [2007] SCSS model. Results show that the Erta Ale melt would be saturated with sulfide at 1610–2640 ppm S for the compositions of Erta Ale melt inclusions and matrix glass, at temperature of 1150°C, and pressure between 1 and 1500 bars. The highest S concentration measured in melt inclusions from Erta Ale is 1220 ppm, lower than sulfide saturation concentrations.

[42] Similarly, the compositions of Masaya melt inclusions and matrix glass indicate SCSS of 1055–1860 ppm from the *Liu et al*. [2007] model for a temperature of 1100°C and pressures between 1 and 1500 bars. *Sadofsky et al*. [2008] report a water content of 1.7 wt % for Masaya melt inclusions, and the highest S concentration measured in melt inclusions from Masaya is 480 ppm, well below sulfide saturation. The predominance of S^{6+} in these relatively oxidized melts (section 5.1) makes it more appropriate to consider the sulfur content at sulfate (i.e., anhydrite) saturation. *Jugo et al*. [2010] demonstrate the SCAS (sulfur content at anhydrite saturation) is ~1.2 wt % at ΔQFM >1.5, similar to that calculated for the Masaya melt (section 5.1). The *Li and Ripley* [2009] model for sulfur content at anhydrite saturation yields saturation concentrations of 3300–7070 ppm, which is far higher than S concentrations observed in the melt. The *Baker and Moretti* [2011] model takes the effect of water into account and gives SCAS of 1620–29,100 ppm for Masaya melts.

[43] *Lee et al*. [2012] argued that Cu content of whole rocks can be used as a tracer of sulfide saturation, with Cu depletion indicating precipitation of sulfides. Masaya lavas have some of the highest Cu contents of any lavas along the Central American arc with an average of ~250 ppm Cu [*Carr and Rose*, 1987], far higher than the depleted values of <50 ppm expected for magmas that have experienced sulfide saturation [*Lee et al*., 2012]. Erta Ale lavas have ~120 ppm Cu [*Zelenski et al*., 2013], which is also elevated and above the range in MORB (40–90 ppm) or bulk continental crust (~30 ppm) [*Lee et al*., 2012]. We thus conclude that neither the Erta Ale melts nor the Masaya melts show any evidence for saturation in S-bearing mineral phases.

[44] In the interpretation presented below, we use the highest measured S concentrations from olivine-hosted melts inclusions from Erta Ale (~1200 ppm S; this study) and Masaya (~500 ppm S) [*Sadofsky et al*, 2008] in assessing sulfur mass balance and isotope fractionation. Olivine crystallization occurs at relatively low pressure at both Erta Ale and Masaya [*Field et al*., 2012; *Walker et al*., 1993]. Water concentrations were measured in Masaya olivine-hosted melt inclusions by *Sadofsky et al*. [2008] who reported a value of 1.7 wt % H_2O, and the major element totals for our melt inclusions from Masaya suggest H_2O contents of 0.5–1.7 wt % (by difference from 100%). These are low water contents for an arc magma with high Ba/La and consistent with low-pressure crystallization of olivine. Similarly, *Field et al*. [2012] measured low concentrations of CO_2 (≤200 ppm) and H_2O (≤1300 ppm) in olivine-hosted melt inclusions, and calculated low pressures (<0.5 kbar) for olivine crystallization. *Field et al*. [2012] report lower S concentration of 205 ppm S in one of their Erta Ale inclusions, similar to the most degassed inclusions from this study (Figure 5c). We cannot discount that some S degassing may have occurred prior to melt inclusion entrapment, but rely on the highest measured S concentrations as the best available constraint on the undegassed S concentration in the Erta Ale and Masaya melts. In particular, the S concentrations in Masaya melt inclusions are low compared to arc basalts with melt inclusions trapped at higher pressure, which typically range ~1000 ppm S [*Wallace and Edmonds*, 2011]. This is also the value used by *Stix* [2007] in modeling magma degassing rate at Masaya, therefore we also consider the case where the undegassed melt at Masaya contains 1000 ppm S.

5.3. Conceptual Model of S Degassing and Primary S Isotope Compositions

[45] Erta Ale and Masaya are both type examples of open system volcanoes that degas persistently with minor eruption of magma. A conceptual model for S degassing at Erta Ale and Masaya is given in Figure 7 with fluxes and isotope compositions for each system. If the highest S concentration measured in melt inclusions is representative of the undegassed S content of the melt, then

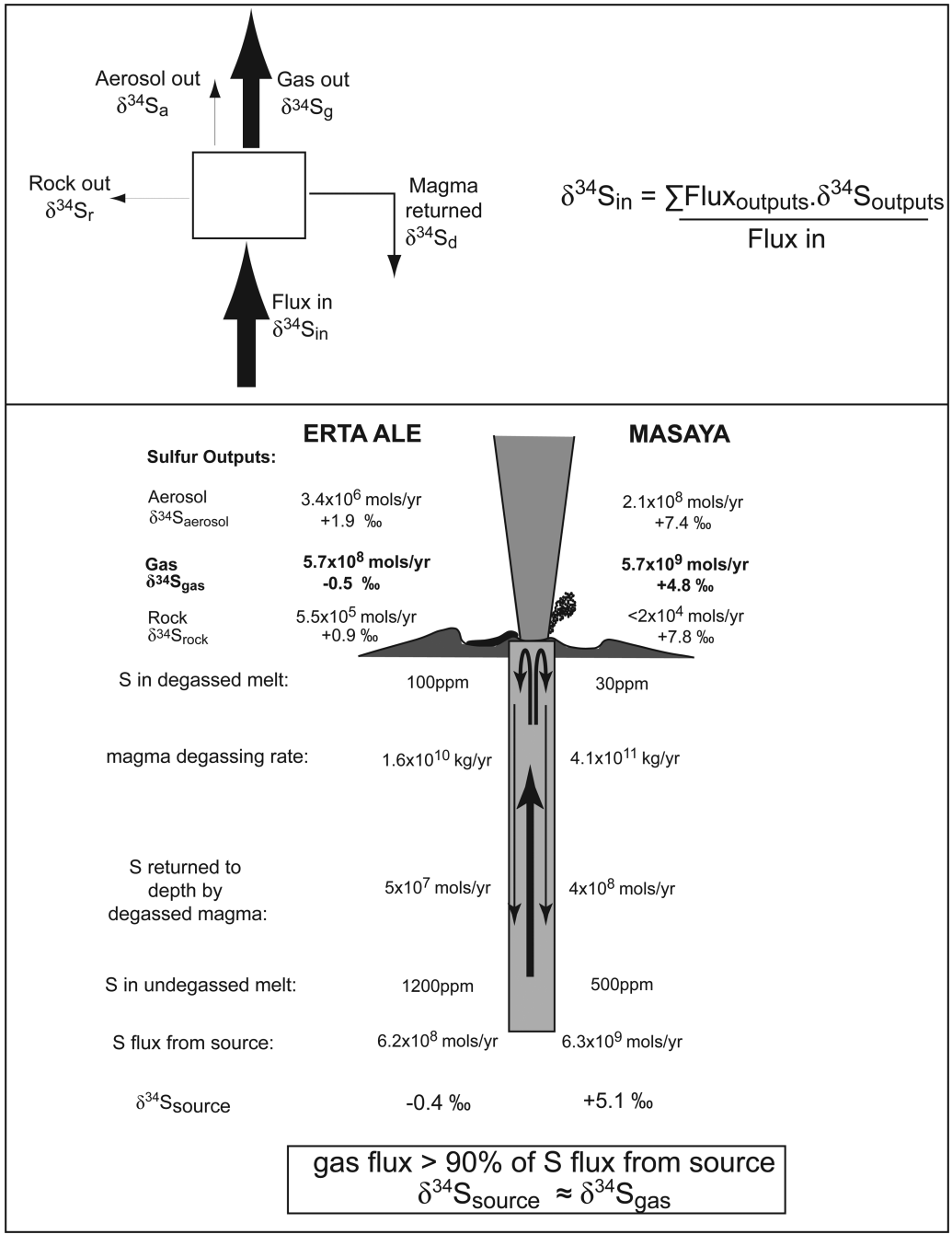

Figure 7. Conceptual model of persistently degassing volcanoes at steady state. (top) A box model for a magmatic system, with arrows scaled to fluxes into and out of the magmatic system. The S flux into the system is from the magma source, the gas emissions dominate the S flux out of the system, the flux of sulfur in rocks (i.e., erupted lava and scoria) is minor, and degassed melt returned to depth by convective degassing is also small. (bottom) The conceptual model of convective degassing, with constraints on S fluxes and S isotope compositions for Erta Ale and Masaya.

magma degassing rates can be calculated from SO_2 fluxes [e.g., *Andres et al.*, 1991; *de Moor et al.*, 2005; *Kazahaya et al.*, 1994; *Pallister et al.*, 2005; *Palma et al.*, 2011; *Stix*, 2007; *Stoiber et al.*, 1986]:

$$Q_m = 100 \frac{M_S}{M_{SO_2}} . \frac{Q_{SO_2}}{\Delta S} \quad (4)$$

where Q_m is the magma degassing rate in kg/s, Q_{SO2} is the measured flux of SO_2 gas in kg/s, ΔS

is the sulfur lost from the melt in wt %, and M_S and M_{SO2} are the molecular masses of S and SO_2, respectively. At Erta Ale, the magma degassing rate is estimated at ~520 kg/s or 1.6×10^{10} kg/yr (using an SO_2 flux of 1.16 kg/s, a melt S content of 1218 ppm S, and a degassed melt content of 100 ppm). The 2010 eruption produced ~6×10^6 m^3 of lava [*Field et al*., 2012] and the 1968–1974 eruptions produced ~9.7×10^6 m^3 [*Oppenheimer and Francis*, 1997], yielding erupted masses of 8.1×10^9 and 1.5×10^{10} kg, respectively (using a vesicularity of 50% [*Field et al*., 2012] and a melt density of 2700 kg/m^3). These masses yield eruption rates of 2.3×10^8 kg/yr (1975–2011) to 4.9×10^8 kg/yr (1968–2011), which are almost 2 orders of magnitude lower than the magma degassing rate. Matrix glass contains ~100 ppm S (section 4.2), resulting in a S flux of 0.7×10^6 mol/yr to 1.8×10^6 mol/yr from the volcano as lava. In comparison, the S flux by degassing of the volcano is almost 3 orders of magnitude higher at ~5.7×10^8 mol/yr and strongly dominates the sulfur output budget. The flux of sulfate aerosol is estimated at 3.4×10^6 mol/yr based on the SO_2 flux and SO_4/SO_2 ratio measured in the plume (Table 3).

[46] The magma degassing rate at Masaya is far higher than at Erta Ale. Using a melt S content of 480 ppm from *Sadofsky et al*. [2008], a degassed melt content of 30 ppm S (section 4.2) and an average SO_2 flux of 1000 tons/d (11.6 kg/s) [*Martin et al*., 2010; *Nadeau and Williams-Jones*, 2009] the magma degassing rate is estimated at ~12,975 kg/s or 4.1×10^{11} kg/yr. Given the variability of SO_2 gas emission from Masaya (3.8–27.6 kg/s; Figure 3), the magma degassing rate may vary between ~4000 and ~29,000 kg/s. If the undegassed melt concentration was 1000 ppm [*Stix*, 2007] then calculated magma degassing rates would be half of that reported above. An insignificant mass of this degassed magma is erupted, with 14 minor explosions since 1950 with minimal ash deposition [*Venzke et al*., 2002]. In order to provide some constraint on the magma eruption rate, we consider the 1772 and 1670 lava flows, which have masses of 2.5×10^9 and 2.0×10^{10} kg [*Venzke et al*., 2002; *Williams*, 1983], yielding a magma eruption rate of 6.7×10^7 kg/yr (for the time period 1670–2011), which is 4 orders of magnitude lower than the magma degassing rate. This large discrepancy dwarfs the uncertainties in the magma degassing rate due to uncertainties in the initial S content. Considering a melt content of 30 ppm after degassing yields a flux of $<2 \times 10^4$ mol/yr S in lava. In comparison, the S gas flux is 5.7×10^9 mol/yr, and that of sulfate aerosols is ~2.1×10^8 mol/yr.

[47] Persistent degassing with minor erupted magma at open vent basaltic volcanoes has been attributed to convective degassing of magma in the conduit [*Kazahaya et al*., 1994; *Palma et al*., 2011; *Shinohara*, 2008]. In open vent basaltic systems such as Erta Ale and Masaya, low-density volatile-rich magma ascends from magma chamber depths into the conduit and vapor bubbles form once volatile saturation is reached due to decrease in pressure. The formation of bubbles further decreases the density of the magma and gas separation occurs in the upper conduit. The degassed magma is denser and bubble poor and descends [*Kazahaya et al*., 1994; *Palma et al*., 2011; *Shinohara*, 2008]. Convective degassing thus allows magma to lose almost all volatiles to the surface through decompression degassing, without eruption of magma.

[48] Figure 7 shows the S mass balance for steady state convective degassing at Erta Ale and Masaya. Undegassed melt enters the base of the conduit system carrying dissolved S (1200 ppm at Erta Ale, 480 ppm at Masaya) from the source. If we consider a volume of undegassed melt rising up the conduit, CO_2-rich bubbles will first nucleate and further drive buoyant rise [e.g., *Shishkina et al*., 2010]. These bubbles grow by diffusion of volatiles from the melt into the bubble as volatiles partition into the gas phase [e.g., *Sparks*, 2003]. Thus, for the case of sulfur, almost all of the S in the volume of melt (>90% based on the difference in S concentration between melt inclusions and matrix glass; note that if a higher undegassed S concentration is used then the calculated extent of S degassing increases) is partitioned into bubbles by diffusion from the melt, and is released to the gas plume by magma-gas separation. At the top of the conduit, the melt has lost >90% of its dissolved S to the gas phase, and the S gas fluxes are constrained by direct measurement (5.7×10^8 mol/yr at Erta Ale, 5.7×10^9 mol/yr at Masaya). Degassed magma (with ~100 ppm S at Erta Ale, ~30 ppm S at Masaya) is denser than volatile-rich melt and sinks by convection. The flux of degassed magma returning to depth is almost the same as the magma degassing rate because insignificant magma is erupted. The mass of S returned to depth by convection is thus calculated at 5×10^7 mol/yr for Erta Ale and 4×10^8 mol/yr for Masaya. These values would decrease if higher undegassed melt S concentrations were adopted.

[49] The total S flux into the base of the system is the sum of S released as gas, S released as aerosol, S returned to depth by convection of degassed magma, and S erupted in rocks. As the S isotope compositions of gas, aerosol, and degassed melt are known, the S isotope composition of the S source (i.e., undegassed melt) can be calculated (Figure 7), but is essentially identical to that of the gas because the vast majority of the S leaves the system as gas. Note that if higher undegassed melt S concentrations are used the only value in the S mass balance that changes is the S returned to depth by degassed magma (because this is calculated from the magma degassing rate), which decreases and thus yields a larger proportion of the total S in the system released as gas.

[50] The S isotope composition of plume gas from Erta Ale is -0.5 ± 0.6‰. Considering mass balance and fluxes of S from eruption of lava and convective descent of degassed melt results in an undegassed melt composition of -0.4‰, which is indistinguishable from the gas composition (Figure 7). At Masaya, plume gas has a value of $+4.8 \pm 0.4$‰, and a mass balance-derived source composition of $+5.1$‰. Thus, at steady state, the sulfur isotope composition of the plume gas is representative of that introduced to the shallow system from the source.

[51] Lacking evidence for significant crustal assimilation in recent eruptive products from either volcano [*Barberi and Varet*, 1970; *Barrat et al*., 1998; *Walker et al*., 1993], the emitted sulfur must ultimately be from subcrustal sources (i.e. mantle or subduction fluids; also see section 5.8). Low-pressure crystallization (<0.5 kbar) is the dominant process of melt differentiation at both volcanoes, with estimated degrees of crystallization at <20% olivine + plagioclase + clinopyroxene [*Field et al*., 2012; *Walker et al*., 1993]. The relative roles of shallow magma convection and time scales of replenishment of shallow tholeiitic magma chambers by parental mantle-derived melts in maintaining persistent gas emissions from open vent volcanoes is not fully resolved [*Wallace and Edmonds*, 2011], though influx of hot volatile-rich melts seems necessary for maintaining convection and gas flux. *Field et al*. [2012] suggested that the 2010 eruption at Erta Ale was driven by replenishment of the magma system by fresh magma. *Walker et al*. [1993] considered periodic influx of mafic magma a necessary condition for maintaining the long-lived and chemically homogenous magma reservoir at Masaya. We therefore assume that the S isotope composition of the gas phase emitted from Erta Ale and Masaya is representative of the composition of S injected into the system from the mantle (carried in melt), although there may be some delay in degassing if S is first stored in a deeper magma chamber before it is released by convective degassing.

[52] At both volcanoes, the isotope composition of scoria, representing the residual S in the melt, has higher δ^{34}S than the gas indicating a degassing fractionation effect. The fractionation effect is larger at Masaya, with observed $\Delta^{34}S_{\text{gas-melt}} \sim -2.6$‰ whereas at Erta Ale the observed difference is smaller at $\Delta^{34}S_{\text{gas-melt}} \sim -1.3$‰.

5.4. Equilibrium Degassing Fractionation Factors

[53] The S isotope compositions of gas and melt can be assessed based on isotopic equilibrium between S species present in the gas and melt. Below, we use degassing fractionation modeling to assess fractionation effects during S degassing at Erta Ale (section 5.5) and Masaya (section 5.6). How S isotopes partition between gas and melt phases during equilibrium degassing is a function of the S species present in the melt (primarily a function of fO_2; Figure 5b) and the S species present in the gas (a function of fO_2, P, T, and fH_2O). The more oxidized forms of S tend to retain the heavy isotope due to relatively stronger covalent bonding compared to bonds with the light isotope such that $\delta^{34}S$ $SO_4^{2-} > SO_2 > S^{2-} \approx H_2S$. Isotopic fractionation is temperature dependent and fractionation factors (α_{x-y} where x and y are different S species) are taken from the experimental results of *Miyoshi et al*. [1984]:

$$1000\ \ln\alpha_{SO_4^{2-}-H_2S} = 6.5\left(10^6/T^2\right) \quad (5)$$

$$1000\ \ln\alpha_{SO_4^{2-}-S^{2-}} = 7.4\ \left(10^6/T^2\right) - 0.19 \quad (6)$$

[54] and the thermodynamic calculations of *Richet et al*. [1977]:

$$1000\ \ln\alpha_{SO_2-H_2S} = 4.7\left(10^6/T^2\right)^2 - 0.5 \quad (7)$$

[55] Combinations of these equations allow:

$$1000\ \ln\alpha_{SO_2-SO_4^{2-}} = 1000\ \ln\alpha_{SO_2-H_2S} - 1000\ \ln\alpha_{SO_4^{2-}-H_2S} \quad (8)$$

$$1000\ \ln\alpha_{SO_2-S^{2-}} = 1000\ \ln\alpha_{SO_2-SO_4^{2-}} - 1000\ \ln\alpha_{S^{2-}-SO_4^{2-}} \quad (9)$$

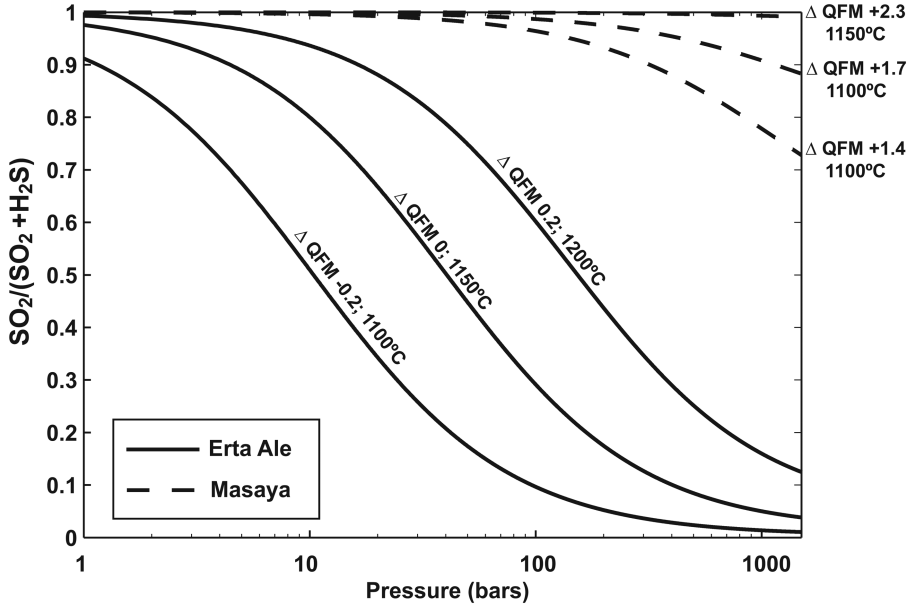

Figure 8. Modeled $SO_2/(SO_2+H_2S)$ as a function of pressure (1–1500 bars) for fO_2 and temperature conditions at Erta Ale and Masaya.

$$1000\ \ln\alpha_{H_2S-S^{2-}} = 1000\ \mathrm{In}\alpha_{SO_4^{2-}-S^{2-}} - 1000\ \mathrm{In}\alpha_{SO_4^{2-}-H_2S} \quad (10)$$

[56] Equilibrium sulfur isotope fractionation between the bulk gas and melt phases (considering the major S species in gas and melt) is given by the equation of *Mandeville et al*. [2009]:

$$\begin{aligned}1000\ \ln\alpha_{gas-melt} = {} & \mathrm{XA}\,1000\ \ln\alpha_{H_2S-SO_4^{2-}} \\ & + \mathrm{XB}\,1000\ \ln\alpha_{SO_2-SO_4^{2-}} \\ & + \mathrm{YB}\,1000\ \ln\alpha_{SO_2-S^{2-}} \\ & + \mathrm{YA}\,1000\ \ln\alpha_{H_2S-S^{2-}}\end{aligned} \quad (11)$$

[57] Where X is the mole fraction SO_4^{2-} dissolved in the melt, Y is the mole fraction of S^{2-} in the melt, A is the mole fraction of H_2S in the gas phase, and B is the mole fraction of SO_2 in the gas phase. A fourth term ($\mathrm{YA}\,1000\ln\alpha_{H_2S-S^{2-}}$) is included in equation (11) for the fractionation between H_2S and S^{2-} (for completeness; not in the original equation of *Mandeville et al*. [2009]), though this term is close to zero at high temperature and was therefore ignored by *Mandeville et al*. [2009]. It is important to note that equation (11) can be rearranged to obtain to the original gas-melt fractionation equation of *Sakai et al*. [1982]:

$$\begin{aligned}1000\ \ln\alpha_{gas-melt} = {} & 1000\ \ln\alpha_{SO_2-S^{2-}} - (1-\mathrm{B}) \\ & 1000\ \ln\alpha_{SO_2-H_2S} - (1-Y)1000\ \ln\alpha_{SO_4^{2-}-S^{2-}}\end{aligned} \quad (12)$$

[58] However, we prefer the more generic form of the gas-melt fractionation equation (equation (11)) because equation (12) was formulated for a system dominated by S^{2-} in the melt and SO_2 in the gas and thus implies that the fractionation between these species (i.e., $1000\ln\alpha_{SO_2-S^{2-}}$) dominates the isotope fractionation between the gas and the melt. This is not the case for highly oxidized melts where the overwhelming majority of S in the melt can exist as S^{6+} (Figure 5b) or systems in which H_2S may be the dominant S gas species.

[59] We assessed equilibrium fractionation factors between melt and gas for Erta Ale and Masaya considering constraints on S speciation in the melt and the degassing temperature. The S speciation in the gas may vary with pressure (see Figure 8), and thus we model the SO_2/H_2S ratio as a function of melt fO_2 and pressure:

$$\begin{aligned}\log(\mathrm{fSO_2/fH_2S}) = {} & \log\mathrm{K} + 1.5\log(fO_2) \\ & - \log(\gamma\mathrm{H_2O}) - \log(\mathrm{XH_2O}) - \log\mathrm{P}\end{aligned} \quad (13)$$

from *Gerlach et al*. [1996], where K is the equilibrium constant for equation (3), which is calculated from:

$$-\Delta\mathrm{G_T} = \mathrm{RT}\ln\mathrm{K} \quad (14)$$

[60] where R is the gas constant and ΔG_T is the Gibbs free energy of reaction at T:

$$\Delta\mathrm{G_T} = -511.89 + 7.318\mathrm{x}10^{-2}\mathrm{T} + 3.3367\mathrm{x}10^{6}\mathrm{T}^{-2} \quad (15)$$

from *Robie and Hemingway* [1995]. The fugacity coefficient for water (γH_2O) in the gas phase is

calculated from *Holland and Powell* [1991], and mole fractions for H_2O (i.e. moles H_2O/total moles gas) in the gas were estimated from direct measurements of gas emissions from Erta Ale (H_20 mole fraction 0.6–0.95) [*Giggenbach and Le Guern*, 1976; *Sawyer et al*., 2008; this study] and Masaya (H_2O mole fraction of 0.85–0.95) [*Burton et al*., 2000; *Martin et al*., 2010].

[61] Experimental studies show that S partitions strongly from the melt into a gas phase at pressures less than ~1.5 kbar [*Lesne et al*., 2011; *Webster and Botcharnikov*, 2011]. These results are consistent with melt inclusion studies, where pressure is estimated from CO_2 and H_2O solubility at Etna [*Spilliaert et al*., 2006] and Stromboli [*Metrich et al*., 2010]. We thus adopt 1.5 kbar as the maximum pressure at which there is a significant proportion of the total S in the melt + gas system in the gas phase. Figure 8 shows the modeled molar ratio of $SO_2/(SO_2+H_2S)$ in the gas phase as a function of pressure, oxygen fugacity, and temperature. At 1 bar, gases at both Erta Ale (ΔQFM = 0.0) and Masaya (ΔQFM = 1.7) are modeled to be strongly dominated by SO_2, which is consistent with the observation that no H_2S was detected in the plumes of either volcano by our sampling method. High-temperature fumarolic gases collected at Erta Ale in 1971 and 1974 have average $SO_2/(SO_2+H_2S)$ ratios of 1.00 and 0.92, respectively [*Giggenbach and Le Guern*, 1976; *Le Guern et al*., 1979], with the highest $SO_2/(SO_2+H_2S)$ ratios corresponding to samples with significant atmospheric O_2. Therefore combustion of H_2S by reaction with atmospheric oxygen [e.g., *Gerlach*, 1980] could further promote SO_2 in plume gases, which is also consistent with oxidation of other reduced gases such as CO and H_2 upon exposure to the atmosphere [*Le Guern et al*., 1979]. However for the conditions at Erta Ale (at ΔQFM = 0, and T = 1150°C) the model shows that the gas phase is dominated by H_2S at pressure greater than 40 bars (Figure 8). For the degassing conditions at Masaya (ΔQFM ≈ 1.7, and T ≈ 1100°C), SO_2 is dominant in the gas even at pressures up to 1500 bars.

5.5. Degassing Fractionation of Sulfur Isotopes at Erta Ale and S Diffusion in Reduced Melt

[62] Figure 9a shows an empirical S isotope fractionation model for open system degassing at Erta Ale. Gas from the Erta Ale plume has a sulfur isotope composition ~1.3‰ lower than that of the degassed scoria. The fraction of S in the gas phase (0.93; lower x axis) is calculated from the S budget for the magmatic system (Figure 7). The isotope composition of the gas plume is -0.5 ± 0.6‰. Scoria (representative of degassed melt) has S concentrations in the matrix glass of 26–218 ppm, and $\delta^{34}S$ values of +0.5‰ to +1.1‰. An initial S concentration of 1200 ppm is used for undegassed melt based on the highest S concentration measured in olivine-hosted melt inclusions. The equations for open system degassing are from *Holloway and Blank* [1994]:

$$\delta^{34}S_{melt} = \left(\delta^{34}S_{source} + 1000\right)\left(F_m^{\left(\alpha_{gas-melt}-1\right)}\right) - 1000 \quad (16)$$

$$\delta^{34}S_{gas} = \left(\delta^{34}S_{source} + 1000\right)\left(F_g^{\left(1/\alpha_{gas-melt}-1\right)}\right) - 1000 \quad (17)$$

[63] The gas is modeled as an accumulated phase derived from steady state convective degassing (section 5.3), calculated by integrating equation (17).

[64] Values for $\alpha_{gas\text{-}melt}$ were varied iteratively to reproduce the compositions of scoria and plume gas. At Erta Ale, $\Delta^{34}S_{gas\text{-}melt}$ is negative (−1.3‰) and therefore values for $\alpha_{gas\text{-}melt}$ must be <1 in order to reproduce the isotope compositions measured in the scoria/degassed melt. The model results in an empirical fractionation factor between gas and melt ($\alpha_{gas\text{-}melt}$) of 0.9991–0.9997.

[65] The measured negative $\Delta^{34}S_{gas\text{-}melt}$ and empirical values for $\alpha_{gas\text{-}melt} < 1$ cannot be reconciled with equilibrium degassing of a melt that is dominated by S^{2-} (Figures 5b and 9b). At equilibrium, the gas phase would be isotopically heavy relative to the melt, the opposite of what is observed at Erta Ale. Figure 9b shows hypothetical equilibrium degassing fractionation curves for constant fO_2 conditions at Erta Ale (i.e., ΔQFM = 0). Three cases are considered for the S speciation in the gas phase (Figure 8): All gas as SO_2 (i.e., low-pressure degassing), all gas as H_2S (i.e., high-pressure degassing), and degassing of equal proportions of SO_2 and H_2S. Under equilibrium degassing conditions the melt would be isotopically lighter than the gas, the opposite of what is observed.

[66] The observation that the scoria is isotopically heavy relative to the plume gas can be explained by kinetic fractionation during S degassing. Sulfur

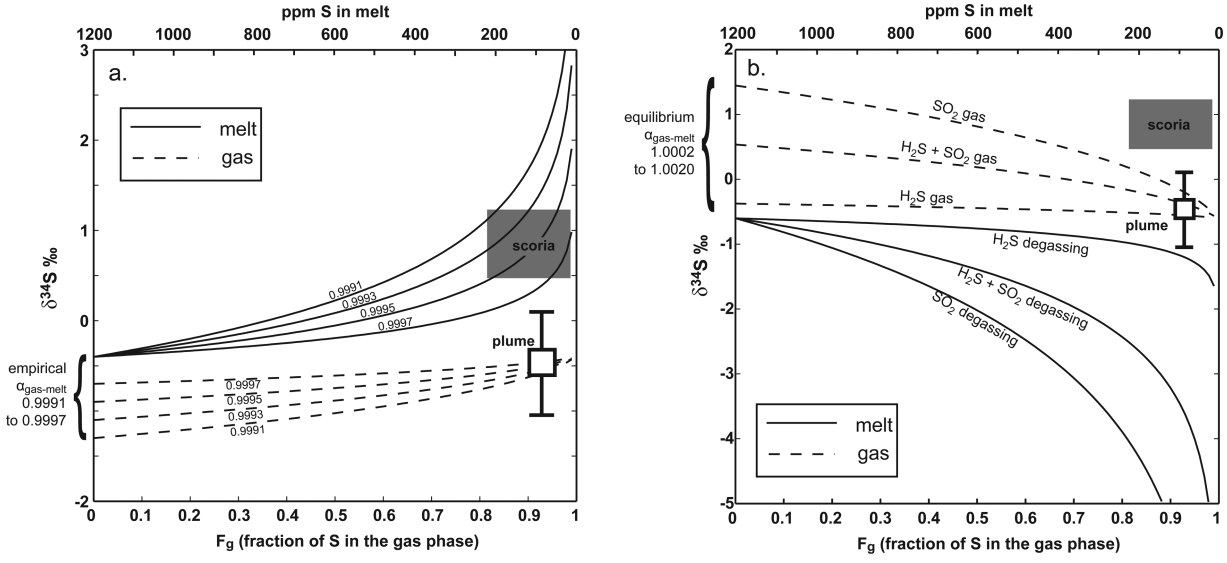

Figure 9. (a) Open system model for degassing fractionation at Erta Ale with $\alpha_{\text{gas-melt}}$ empirically fit to reproduce isotope compositions of plume gas and scoria, with a source composition of −0.4‰. The gas is modeled as an accumulated phase. The fraction of S in the gas phase (i.e., value of F for plume gas) is calculated from mass balance (see section 5.3 and Figure 7). The melt is modeled with an initial S content of 1200 ppm, and the field for scoria is shown as a gray box. Values for $\alpha_{\text{gas-melt}}$ have to be <1 in order to reproduce the compositions of scoria and are estimated to be between 0.9991 and 0.9997. (b) Erta Ale degassing fractionation model with curves for equilibrium degassing fractionation between a melt with $S^{6+}/\sum S = 0.01$ (ΔQFM 0.0). Cases are shown for degassing of pure SO_2, pure H_2S and gas containing equal proportions of SO_2 and H_2S. The isotope compositions of scoria and plume gas cannot be reproduced by equilibrium degassing fractionation.

diffusion is slow in basaltic melts (10^{-12} m^2 s^{-1} at 1300°C in anhydrous basalt) [*Behrens and Stelling*, 2011; *Freda et al.*, 2005], about an order of magnitude lower than H_2O diffusion, and about a factor of two lower than CO_2, and is amongst the slowest species to diffuse through melts. Diffusion plays a fundamental role during volatile partitioning into the gas phase [*Behrens and Stelling*, 2011; *Sparks*, 2003; *Sparks et al.*, 1994]. The light isotope of S has higher translational velocity than the heavy isotope at all temperatures. The difference in translational velocity between ^{32}S and ^{34}S for the ideal gas case is calculated from

$$\text{K.E.} = \frac{1}{2}mv^2 \tag{18}$$

where K.E. is the kinetic energy, m is mass, and v is velocity, such that:

$$\frac{v_2}{v_1} = \sqrt{m_1/m_2} \tag{19}$$

[67] which determines the maximum translational (kinetic) isotopic fractionation factor:

$$\alpha_{kinetic} = \sqrt{\frac{m_1}{m_2}} \tag{20}$$

[68] Table 6 shows theoretical kinetic fractionation factors between S species considered relevant to S diffusion in melts. For the end-member case of pure translational fractionation between $^{32}S^{2-}$ and $^{34}S^{2-}$, a large effect ($\alpha_{\text{kinetic}} = 0.970$) would be expected and this kinetic fractionation is

Table 6. Theoretical Kinetic Fractionation Effects Between S Species in Basaltic Melts Compared to Empirical Estimations at Erta Ale and Masaya

	α_{kinetic}	1000 lnα
Theoretical		
$^{32}S^{2-}$–$^{34}S^{2-}$	0.970	−30
$Fe^{32}S$–$Fe^{34}S$	0.989	−11
$^{32}SO_4$–$^{34}SO_4$	0.990	−10
$Ca^{32}SO_4$–$Ca^{34}SO_4$	0.993	−7
$Fe^{32}S$–$Ca^{34}SO_4$	0.797	−226
$^{32}S^{2-}$–$^{34}SO_4^{2-}$	0.571	−560
Gas-Melt ($\alpha_{empirical}/\alpha_{equilibrium}$)		
Erta Ale lower	0.9971	−2.9
Erta Ale upper	0.9995	−0.5
Masaya	1	0

independent of temperature. At Erta Ale, S^{2-} is dominant in the melt ($S^{6+}/\sum S < 0.07$) and diffusion of S^{2-} through the melt may thus dictate whether chemical and isotopic equilibrium is obtained between gas and melt. S^{2-} complexes with Fe^{2+} in reduced melts [e.g., *Carroll and Webster*, 1994; *Haughton et al*., 1974; *Klimm et al*., 2012; *O'Neill and Mavrogenes*, 2002; *Wallace and Carmichael*, 1992; *Wilke et al*., 2011], thus the effective size and mass of the diffusing species may be much larger than that of S^{2-} [*Behrens and Stelling*, 2011]. A very large kinetic fractionation is plausible between S^{2-} and SO_4^{2-} diffusion in melts with $\alpha_{kinetic} = 0.571$ (Table 6).

[69] The empirically calculated values for $\alpha_{gas\text{-}melt}$ of 0.9991–0.9997 for Erta Ale are closer to unity than those derived for the theoretical cases of S^{2-}, FeS, or S^{2-}/SO_4^{2-} kinetic fractionation, as has to be the case for diffusion through a complex medium such as melt [*Schauble*, 2004]. Sulfur diffusion is a complex processes involving the breaking and reforming of bonds with cations in the melt and debate still surrounds the effect of melt S speciation (i.e., S^{2-} versus SO_4^{2}) in controlling S diffusion [*Behrens and Stelling*, 2011].

[70] Our results show signs of significant kinetic fractionation related to slow S diffusion in melts at Erta Ale. This isotopic fractionation effect is observable due to the reduced nature of the Erta Ale melt. Because S^{2-} is the dominant dissolved S species, equilibrium and kinetic effects work in opposite directions. The equilibrium effect favors ^{34}S in the gas (Figures 1 and 9b), whereas the kinetic effect favors ^{32}S in the gas. At Erta Ale, the kinetic effect dominates over the equilibrium effect.

[71] The relative effects of equilibrium versus kinetic fractionation can be considered based on [e.g., *Schauble*, 2004]:

$$\alpha_{gas-melt} = \alpha_{equilibrium} \times \alpha_{kinetic} \quad (21)$$

[72] The empirical (modeled) $\alpha_{gas\text{-}melt}$ of 0.9991–0.9997 (Figure 9a) and range in calculated $\alpha_{equilibrium}$ values of 1.002–1.0002 (Figure 9b) result in calculated $\alpha_{kinetic}$ values of 0.9971–0.9995 (Table 6). However, Figure 8 shows that H_2S is the dominant gas species for the a large portion of the pressure range where S degassing occurs (i.e., 100–1000 bars) [*Lesne et al*., 2011]. This tends to minimize the equilibrium degassing fractionation effect (Figure 9b), and thus the kinetic effect as well (equation (21)). Considering reasonable degassing conditions (degassing of S at <1.5 kbar, with the fraction of S remaining in the melt as a linear function of P), most of the S lost from the melt was degassed at $P > 50$ bars, with "effective" H_2S degassing accounting for >70% of the degassing experienced by the melt. Rapid re-equilibration between SO_2 and H_2S with decreasing pressure is achieved in the gas phase at magmatic temperatures [*Giggenbach*, 1987; *Taran et al*., 1995], resulting in high SO_2/H_2S ratio in the gases released at the surface. At $SO_2/(SO_2+H_2S)$ in the gas equal to 0.1 and $S^{6+}/\sum S$ in the melt of 0.01, $\alpha_{equilibrium}$ is calculated at 1.0004 (equation (11)). Utilizing equation (21) and the best fit for $\alpha_{empirical}$ of 0.9995 (Figure 9), our best estimate for $\alpha_{kinetic}$ is 0.9991, which we attribute to the relative diffusivities of $^{32}S^{2-}$ and $^{34}S^{2-}$ (or ionic complexes thereof).

[73] Sulfur diffusion coefficients are available for basaltic melts from *Freda et al*. [2005]. The diffusion "rate" (change in diffusion distance over time) can be approximated from [*Zhang*, 2010]:

$$\frac{dx}{dt} = 0.5\sqrt{Dt} \quad (22)$$

where dx/dt is the change in diffusion distance over time, D is the diffusion coefficient in m^2/s, and t is time in seconds. For t from 10^{-5}–10^{5} s, dx/dt is in the range of 10^{-4}–10^{-9} m/s. In comparison, the measured velocity of large bubbles bursting at the surface of the Erta Ale lava lake by *Bouche et al*. [2010] was 4–7 m/s, who also estimated that the conduit feeding the lava lake is ~3 m in radius. Considering the magma degassing rate of 520 kg/s (0.2 m^3/s at a density of 2700 kg/m3, section 5.3) and simple piston flow up a conduit of 3 m radius requires melt velocities of $\sim 10^{-2}$ m/s. Thus, bubbles have higher velocity than melt and low S diffusion prevents equilibration between gas and melt during magma ascent at Erta Ale. This dynamic degassing promotes a kinetic isotopic fractionation effect, which dominates over equilibrium fractionation. The kinetic effect can be observed because kinetic and equilibrium fractionation work in opposite directions due to the reduced nature of the melt.

5.6. Degassing Fractionation at Masaya

[74] The oxygen fugacity at Masaya is typical of arc magmas and sulfate is the dominant S species in the melt (section 4.3). Equilibrium degassing of SO_2 from a melt with $S^{6+}/\sum S > 0.66$ results in a

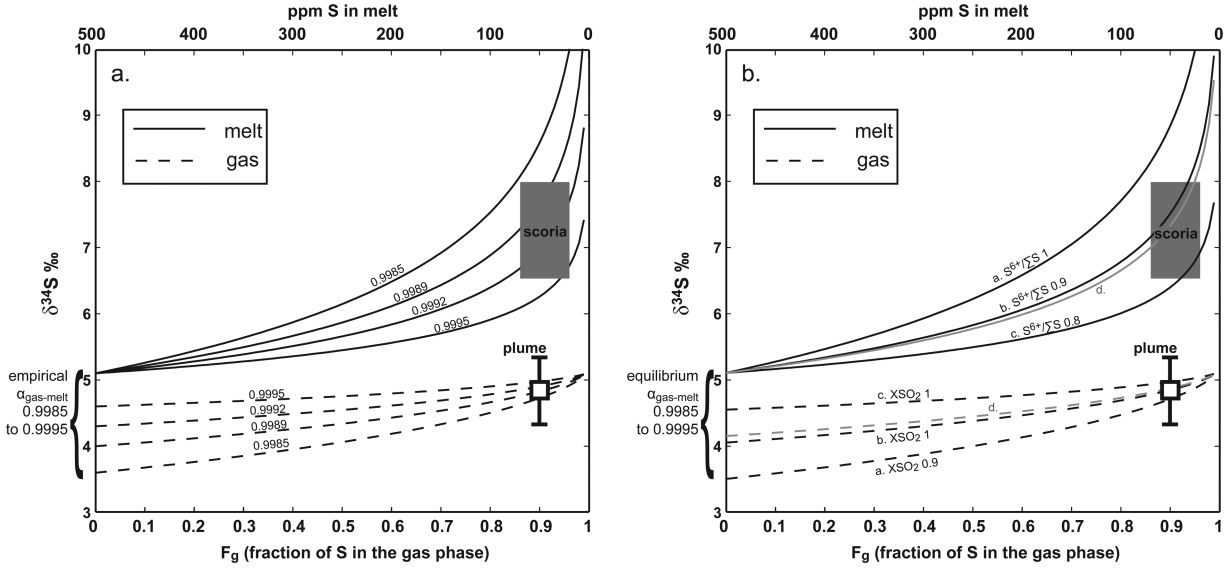

Figure 10. (left) Open system model for degassing fractionation at Masaya with $\alpha_{\text{gas-melt}}$ empirically fit to reproduce isotope compositions of plume gas and scoria, with a source composition of +5.1‰. The gas is modeled as an accumulated phase. The fraction of S in the gas phase (i.e., value of F for plume gas) is calculated from mass balance (see section 5.3 and 79). The melt is modeled with an initial S content of 500 ppm, and the field for scoria is shown as a gray box. Values for $\alpha_{\text{gas-melt}}$ are estimated to be between 0.9985 and 0.9995. (right). Masaya degassing fractionation model for equilibrium degassing between (a) melt with $S^{6+}/\sum S = 1$ and gas $SO_2/SO_2+H_2S = 0.9$, (b) $S^{6+}/\sum S = 0.9$ and pure SO_2, and (c) $S^{6+}/\sum S = 0.8$ and pure SO_2. These conditions are valid for a magmatic system with ΔQFM 1.3–2.1 and pressure <1.5 kbar. The isotope compositions of scoria and plume gas are consistent with equilibrium degassing fractionation. (d) The gray curve shows the case for combined equilibrium and kinetic fractionation with $\alpha_{\text{kinetic}} = 0.9996$, $S^{6+}/\sum S = 0.8$ and SO_2 gas. The range in system constraints does not exclude the possibility that a kinetic effect contributes to the fractionation between melt and gas at Masaya. If kinetic fractionation occurs at Masaya it is not possible to distinguish it from equilibrium fractionation because both favor melt with higher $\delta^{34}S$ in the melt.

fractionation factor <1 (i.e., gas lighter than melt). Thus, the observed negative $\Delta_{\text{gas-melt}}$ at Masaya is generally consistent with degassing from an oxidized magma. Figure 10 (left) shows modeling results with empirical values of $\alpha_{\text{gas-melt}}$ of 0.9985–0.9995, which reproduce the isotope compositions of plume gas and scoria from a source with $\delta^{34}S + 5.1‰$ (Figure 7). These fractionation factors are consistent with equilibrium degassing fractionation of oxidized melt in which S^{6+} is the dominant S species in the melt. Figure 10 (right) shows that the isotope compositions of scoria and plume gas can be reproduced with equilibrium degassing conditions consistent with the oxygen fugacity of the Masaya melt ($\Delta QFM > +1.3$ and $S^{6+}/\sum S > 0.7$; see Table 4 and section 5.1) and a gas phase dominated by SO_2 ($SO_2/(H_2S+SO_2) > 0.9$; see Figure 8 and section 5.4).

[75] However, for magmas with S^{6+} as the dominant S-melt species equilibrium fractionation and kinetic fractionation both favor melt with higher $\delta^{34}S$ than the gas. Gray curves labeled "d" in Figure 10 (right) show the case in which a kinetic fractionation effect is superimposed on equilibrium degassing fractionation. The isotope compositions of plume gas and scoria can be reproduced with a kinetic effect, however this would suggest that the melt at Masaya is at the low end of the fO_2 range calculated for melt inclusions and matrix glass. This may be the case if the matrix glasses have experienced posteruption oxidation due to interaction with the atmosphere or that melt inclusions from Masaya may have been affected by Fe^{2+} diffusion through the olivine host crystals (section S2). Though the case for kinetic fractionation Erta Ale is strong, it is far more ambiguous at Masaya due to the fact that both kinetic and equilibrium effects favor gas with $\delta^{34}S$ lower than that in the melt.

[76] It is necessary to consider the conditions that could favor isotopic equilibrium at Masaya versus kinetic degassing at Erta Ale. Experimental estimates of the effect of water on S diffusion in basaltic melt show that S diffusion is higher by a

factor of three to seven in H_2O-rich melts [*Freda et al*., 2005]. Considering that Masaya melt inclusions have about a factor of 10 higher H_2O content than Erta Ale melt inclusions [*Field et al*., 2012; *Lesne et al*., 2011], S diffusion is expected to be more rapid in Masaya melts, perhaps promoting equilibration with the gas phase. Shorter diffusion pathways would also impede kinetic fractionation effects, so higher bubble to melt ratio at Masaya could provide a plausible explanation for the lack of observable kinetic effects.

[77] A further consideration is differences in the dynamics of degassing at Masaya versus Erta Ale. Masaya is thought to have a conduit-fed shallow magma reservoir at ~1 km depth based on geophysical studies [*Métaxian et al*., 1997; *Stix*, 2007; *Williams-Jones et al*., 2003]. Sulfur input from the conduit into the shallow magma reservoir is balanced by steady state degassing at the vent [*Stix*, 2007]. The plumbing system at Masaya may therefore result in a longer gas residence time at low pressure allowing equilibration between the gas and melt.

5.7. Implications for S Degassing and Redox Conditions of Melts

[78] Sulfur plays an important role in the oxidation state of magmas [*Anderson and Wright*, 1972; *Behrens and Stelling*, 2011; *Burgisser and Scaillet*, 2007; *Kelley and Cottrell*, 2009, 2012; *Klimm et al*., 2012; *Lee et al*., 2012]. Sulfur degassing may oxidize or reduce melts [*Burgisser and Scaillet*, 2007; *Kelley and Cottrell*, 2012; *Metrich et al*., 2009] depending on the S speciation in gas and melt phases. Oxygen fugacity is a major controlling variable determining the redox states of S in the melt and the gas, but the fO_2 of a magma may also be modified by open system degassing [e.g., *Burgisser and Scaillet*, 2007]. Erta Ale is an important natural laboratory for testing these hypotheses because it is one of the few localities where high-temperature gases and pristine scoria can be sampled. Our data show that melt inclusions and matrix glasses have indistinguishable fO_2 of ΔQFM 0.0 ± 0.3 (Table 4 and Figure 6). This result is in close agreement with fO_2 calculated from CO_2/CO ratios (22.0 ± 1.6; ΔQFM -0.2 ± 0.1) in high-temperature Erta Ale gas samples of *Giggenbach and Le Guern* [1976], our gas samples after correction for reaction with air ($CO_2/CO = 27.3$; ΔQFM -0.1; Table 5) as well as fO_2 calculated from two-oxide thermobarometery for more evolved magmas from the Erta Ale suite [*Bizouard et al*., 1980] (Figure 6). The Erta Ale magma system shows no change in fO_2 with degassing or crystallization (also see section 5.1).

[79] Though SO_2 is strongly dominant in the Erta Ale plume, degassing at higher pressure that favors H_2S must be dominant otherwise reduction of the melt, dominated by S^{2-}, would be expected from:

$$6Fe^{3+}_{melt} + S^{2-}_{melt} \leftrightarrow S^{4+}_{gas} + 6Fe^{2+}_{melt} \quad (23)$$

[80] Thus, degassing of 1 mol of SO_2 would result in reduction of 6 mol of Fe^{3+} and loss of 500 ppm S from the melt would reduce the $Fe^{3+}/\sum Fe$ in the melt to ~0.02 (ΔQFM ~ −3.5), which is not observed. Rather, H_2S degassing and gas re-equilibration to SO_2 takes place at low pressure via the "gas buffer" reaction [*Giggenbach*, 1987; *Taran et al*., 1995]:

$$H_2S + 2H_2O \leftrightarrow SO_2 + 3H_2 \quad (24)$$

[81] Thus, S speciation in the gas phase is strongly pressure dependent (because the right hand side of equation (24) has more moles than the left hand side), and H_2S degassing from a melt with S^{2-} results in no redistribution of electrons. Degassing of H_2S from a melt with S^{2-} also results in minimization of the equilibrium isotope fractionation effect (Figure 9b), which allows us to recognize the effect of diffusive S degassing from the melt through stable isotope geochemistry at Erta Ale. Oxidation of H_2S to SO_2 during high-temperature mixing with air is another process that produces high SO_2/H_2S in the emitted gas at Erta Ale. It is however important to note that as long as no (or negligible) S is lost from the gas phase (i.e. negligible loss to aerosol deposition) the isotope composition of the bulk gas is not affected.

[82] The high-fO_2 conditions of the Masaya magma promotes SO_2 as the dominant gas species, even at pressure >500 bar (Figure 8). Considering the case with SO_2 as the only S gas species at Masaya, constant $Fe^{3+}/\sum Fe$ can be maintained in the melt if S degassing occurred by:

$$0.75S^{6+}_{melt} + 0.25S^{2-}_{melt} \leftrightarrow S^{4+}_{gas} \quad (25)$$

[83] Degassing of SO_2 from a melt with $S^{6+}/\sum S > 0.75$ results in oxidation of Fe^{2+} (if no other buffers are present). For example:

$$0.875S^{6+}_{melt} + 0.125S^{2-}_{melt} + Fe^{2+}_{melt} \leftrightarrow S^{4+}_{gas} + Fe^{3+}_{melt} \quad (26)$$

[84] This could provide a reasonable explanation for the fact that the Masaya matrix glass is slightly more oxidized (in terms of $Fe^{3+}/\sum Fe$) than melt inclusions, though it is equally plausible that the matrix glass experienced oxidation due to interaction with atmospheric oxygen. However, the salient point is that any melt with $S^{6+}/\sum S > 0.75$ will oxidize Fe^{2+} [*Metrich et al*., 2009] due to S degassing if S^{6+} and S^{2-} contribute to the gas phase in the same proportion in which they exist in the melt. However, if diffusion of S^{2-} controls S degassing (i.e., diffuses through melt faster than SO_4^{2-}), then melt with $S^{6+}/\sum S > 0.75$ can become more reduced by S degassing.

5.8. Implications for S Isotope Fractionation and S Sources in Magmatic Systems

[85] Previous studies of S isotope compositions of arc rocks have argued that degassing is unlikely to significantly alter their isotope compositions [*Alt et al*., 1993; *de Hoog et al*., 2001]. In recent years, improvements in understanding the relationship between fO_2 and S speciation in melts through advances in XANES analysis [*Jugo et al*., 2010; *Metrich et al*., 2009] show that oxidized melts typical of arc basalts ($\Delta QFM > +1$) are dominated by dissolved sulfate (S^{6+}) to a greater extent than earlier research indicated [*Nilsson and Peach*, 1993; *Wallace and Carmichael*, 1992, 1994]. *Jugo et al*. [2010] and *Wilke et al*. [2011] show that the transition from sulfide to sulfate in melts occurs over a narrower range in fO_2 ($S^{6+}/\sum S$ from 0.1 to 0.9 in $\sim$ 1 log unit) than previously thought ($S^{6+}/\sum S$ from 0.1 to 0.9 in $\sim$ 2 log units) [*Jugo et al*., 2005]. The experimental results of *Jugo et al*. [2010] show that basaltic melts have higher $S^{6+}/\sum S$ at lower fO_2 compared to previous results, which has significant implications for S isotope fractionation during basaltic degassing.

[86] Our equilibrium degassing modeling shows that melts at redox conditions of $\Delta QFM > +1.2$ (i.e. with $S^{6+}\sum S_{melt} > 0.67$) will evolve to higher $\delta^{34}S$ values at any reasonable pressure (1–1500 bars) and $SO_2/(SO_2 + H_2S)$ ratio (0–1). We have demonstrated that in the case of diffusive S degassing, kinetic isotopic fractionation effects must also be considered. Thus, degassing fractionation is likely to affect most basaltic melts/rocks that have lost a significant portion of their original S to the vapor phase, and degassing under most reasonable fO_2 and pressure conditions results in preferential retention of the heavy isotope in oxidized melt. We note that the observed $\Delta^{34}S_{gas\text{-}melt}$ at Masaya is -2.6‰, and that the total range in S isotope compositions of primary products spans $\sim$4‰. In this regard, it is important to note that arc basalts and andesites span a sulfur isotope range of 0‰ to $\sim$ +10‰ [*Marini et al*., 2011]. Our sulfur budget assessment of output fluxes from Masaya (Figure 7), an arc volcano with very high Ba/La and slab fluid signature [*Carr et al*., 1990; *Carr and Rose*, 1987] and no evidence for saturation in any S-bearing mineral phases (section 5.2), indicates a source isotope composition of $\sim$+5.1‰ (Figure 7).

[87] Recent eruptive products from both Masaya and Erta Ale show no geochemical evidence for crustal contamination [*Barberi and Varet*, 1970; *Barrat et al*., 1998; *Walker et al*., 1993]. Crustal sources of sulfur are an unlikely explanation for the clearly distinct primary S isotope compositions observed at Erta Ale and Masaya (i.e., -0.4‰ and +5.1‰, respectively) given the similarity in crustal thickness (i.e., 20 ± 2 km at Erta Ale [*Hammond et al*., 2011] versus 25 ± 4 km at Masaya [*MacKenzie et al*., 2008]). Furthermore, sulfate-rich evaporitic deposits (up to 1000 m in thickness) are common in the Afar region near Erta Ale [*Bosworth et al*., 2005] providing an abundant potential source of isotopically heavy S (close to that of seawater sulfate (i.e., +21‰). Seawater sulfate is also fixed in the altered oceanic crust [e.g., *Alt*, 1995] at oceanic spreading centers (such as the Afar triple junction) by hydrothermal circulation providing an additional potential source of isotopically heavy crustal sulfur. The Dallol hydrothermal system located to the north west of Erta Ale serves as an example of modern vigorous hydrothermal activity in the region [*Darrah et al*., 2013]. Yet, high $\delta^{34}S$ values are not observed at Erta Ale. Rather, elevated S isotope compositions are observed at Masaya where the crust is composed of accreted arc rocks [*MacKenzie et al*., 2008] and acidic volcanic rocks [*Walker et al*., 1993], which do not provide an obvious rich source of isotopically heavy S. Therefore, we discount crustal S as the cause of the distinct S isotope compositions observed at Erta Ale and Masaya. Rather, the positive S isotope compositions observed at Masaya is attributed to its tectonic setting on a subduction zone.

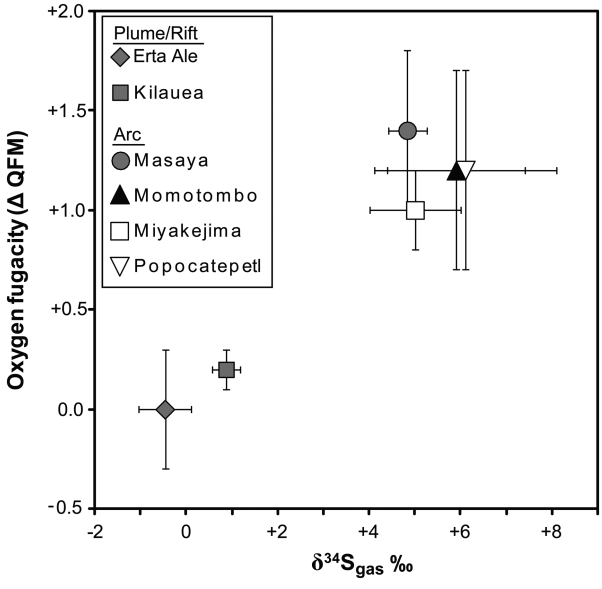

Figure 11. Magmatic oxygen fugacity (ΔQFM) versus gas sulfur isotope compositions for some typical arc volcanoes compared to plume/rift volcanoes. High δ^{34}S values in arc products are attributed to recycling of oxidized sulfur (subducted sulfate) through subduction zones [*Alt et al*., 1993; *de Hoog et al*., 2001; *de Moor et al*., 2010; *Mandeville et al*., 2010, 1998, 2009; *Ueda and Sakai*, 1984]. Data sources: Masaya and Erta Ale—this study; Kilauea: gas δ^{34}S values from *Sakai et al*. [1982], fO_2 for gases and rocks from *Gerlach* [1993]; Momotombo: gas δ^{34}S values from *Menyailov et al*. [1986], fO_2 for gases and rocks estimated from *Benhamou et al*. [1988]; Miyakejima: gas δ^{34}S from *Ohba et al*. [2008] and magmatic fO_2 from reference therein [*Yasuda et al*., 2001]; Popocatepetl: gas δ^{34}S from *Goff et al*. [1998] corrected for sampling fractionation effects according to *Ohba et al*. [2008] and magmatic fO_2 estimated from *Witter et al*. [2005].

[88] The average isotope compositions of Masaya plume gas is +4.8‰ and within error of the calculated source isotope composition of +5.1‰ because the majority of the S input is released as S gas (Figure 7). Thus, for the case of open vent volcanoes we consider magmatic gases to be more representative of the primary S isotope composition than scoria or lavas. High-temperature gas samples from Momotombo (Ba/La > 100) [*Carr and Rose*, 1987], located S of Masaya, have δ^{34}S values of +4.2 to +6.8‰ [*Menyailov et al*., 1986] (comparing well with our Momotombo gas value of +6.2‰; see section 3.2) and high-temperature SO_2 from Poas volcano in Costa Rica has δ^{34}S values of ~+7‰ [*Rowe*, 1994]. The SO_2 flux from Masaya represents ~23% of the total SO_2 flux from the Central American arc [*Hilton et al*., 2002; *Mather et al*., 2006b] and we thus consider a value of +5‰ to be a reasonable representative of S emitted from the Central American arc segment.

[89] *Marini et al*. [2011] suggested through a model-driven reanalysis of published isotope compositions that magmatic differentiation processes (i.e., degassing and crystallization) from a typical mantle source with δ^{34}S ~ 0 can account for the S isotope variation exhibited by volcanic rocks, gases, and mineral phases. Here, we show that plume gases from an open vent arc volcano, where S gases strongly dominate the total output from the magma system and no sulfide saturation or crustal contamination is evidenced, exhibit source isotope compositions that fall well above the value of 0 ± 2‰ adopted by *Marini et al*. [2011] for the mantle. The results of this study therefore support previous research attributing high δ^{34}S values observed in arc products to recycling of oxidized sulfur (subducted sulfate) through subduction zones [*Alt et al*., 1993; *de Hoog et al*., 2001; *de Moor et al*., 2010; *Mandeville et al*., 2010, 1998, 2009; *Ueda and Sakai*, 1984]. Figure 11 shows the relationship between magmatic oxygen fugacity (relative to the QFM buffer of *Frost* [1991]) and sulfur isotope compositions of volcanic gases (plumes and fumaroles) at plume/rift volcanoes and arc volcanoes, suggesting that recycled oxidized sulfur may play an important role in determining the oxygen fugacity of arc products.

6. Conclusions

[90] The isotope compositions of S sources at Erta Ale and Masaya are −0.4‰ and +5.1‰, respectively. Plume gases at each volcano are close representatives of their source isotope compositions because the vast majority of S output from open vent volcanoes occurs as gas emissions. Degassed scoria have higher δ^{34}S values than plume gas at both volcanoes, despite the fact that Erta Ale melts are dominated by S^{2-} and Masaya melts are dominated by S^{6+}. For the fO_2 and temperature of degassing at Erta Ale, equilibrium degassing cannot be reconciled with the S isotope compositions of plume gas and scoria. Rather, a kinetic isotope fractionation effect is required, which promotes retention of the heavy isotope (due to lower translational velocity) in the melt. This effect is related to relative diffusivities of ^{32}S and ^{34}S (or ionic complexes thereof) and diffusion-controlled S degassing during dynamic magma convection.

[91] We find minimal difference in Fe oxidation state (as measured by Fe XANES) between melt inclusions and matrix glass at Erta Ale indicating minimal change in fO_2. Sulfur in the melt at Erta Ale is dominated by S^{2-} (as measured by S XANES), and the dominance of H_2S degassing (rather than SO_2 degassing) is inferred based on thermodynamic modeling showing that H_2S is the dominant gas exsolved from the Erta Ale melt at pressure > 50 bars. Rapid gas-phase re-equilibration of H_2S to SO_2 occurs as a function of depressurization (with fO_2 maintained at $\Delta QFM = 0$), which accounts for the observation that SO_2 (rather than H_2S) is emitted from the vent.

[92] The isotope compositions of the Masaya plume and scoria are consistent with equilibrium degassing of an oxidized arc magma. However, a small kinetic isotope fraction effect during degassing cannot be ruled out. Equilibration between gas and melt may be related to higher water content in the melt or longer gas residence time in the magma. The isotope composition of the Masaya magma source ($\sim$+5‰) is higher than that of ambient mantle (0.3 ± 0.5‰) [*Sakai et al.*, 1984], consistent with a significant contribution of subducted sulfate to the mantle wedge at the Central American arc. Sulfate-rich fluids released from subducted slabs can oxidize the subarc mantle as reflected by S isotope compositions and oxygen fugacities of arc products.

Acknowledgments

[93] This research was made possible by the National Science Foundation through grant EAR1049891 (TF); and by a NASA Earth and Space Science Fellowship to JMdM/PLK (Planet09F-0044). We also acknowledge support through grants EAR/IF - 0743540 (TF), EAR-0841006 (EC) and EAR-0841108 (KAK). Viorel Atudorei, Vitchko Tsanev, Mike Spilde, and Paul Burger are thanked for analytical and technical assistance. We gratefully acknowledge the European Synchrotron Radiation Facility (ID21) for providing beamtime. Use of the National Synchrotron Light Source (X26A) was supported by DOE under Contracts No. DE-AC02-98CH10886 and DE-FG02-92ER14244. Jan De Hoog and an anonymous reviewer are thanked for thoughtful comments that improved this work. Charlie Mandeville and Chip Shearer are gratefully acknowledged for serving on the PhD committee of the first author and for reviewing a previous version of this manuscript.

References

Allen, A. G., C. Oppenheimer, M. Ferm, P. J. Baxter, L. A. Horrocks, B. Galle, A. J. S. McGonigle, and H. J. Duffell (2002), Primary sulfate aerosol and associated emissions from Masaya Volcano, Nicaragua, *J. Geophys. Res.*, *107*(D23), 4682, doi:10.1029/2002JD002120.

Alt, J. C. (1995), Sulfur isotopic profile through the oceanic-crust—Sulfur mobility and seawater-crustal sulfur exchange during hydrothermal alteration, *Geology*, *23*, 585–588.

Alt, J. C., W. C. Shanks III, and M. C. Jackson (1993), Cycling of sulfur in subduction sones—The geochemistry of sulfur in the Mariana-island arc and back-arc trough, *Earth Planet. Sci. Lett.*, *119*, 477–494.

Anderson, A. T., and T. L. Wright (1972), Phenocrysts and glass inclusions and their bearing on oxidation and mixing of basaltic magmas, Kilauea Volcano, Hawaii, *Am. Mineral.*, *57*, 188–216.

Andres, R. J., and A. D. Kasgnoc (1998), A time-averaged inventory of subaerial volcanic sulfur emissions, *J. Geophys. Res.*, *103*, 25,251–25,261.

Andres, R. J., W. I. Rose, P. R. Kyle, S. deSilva, P. Francis, M. Gardeweg, and H. M. Roa (1991), Excessive sulfur-dioxide emissions from Chilean Volcanos, *J. Volcanol. Geotherm. Res.*, *46*, 323–329.

Backnaes, L., and J. Deubener (2011), Experimental Studies on sulfur solubility in silicate melts at near-atmospheric pressure, in *Sulfur in Magmas and Melts: Its Importance for Natural and Technical Processes*, edited by H. Behrens and J. D. Webster, pp. 143–165, The Mineral. Soc. of Am., Chantilly, Va.

Baker, D. R., and R. Moretti (2011), Modeling the solubility of sulfur in magmas: A 50-year old geochemical challenge, in *Sulfur in Magmas and Melts: Its Importance for Natural and Technical Processes*, edited by H. Behrens and J. D. Webster, pp. 167–213, The Mineral. Soc. of Am., Chantilly, Va.

Banin, A., F. X. Han, I. Kan, and A. Cicelsky (1997), Acidic volatiles and the Mars soil, *J. Geophys. Res.*, *102*, 13,341–13,356.

Barberi, F., and J. Varet (1970), The Erta Ale volcanic range, *Bull. Volcanol.*, *34*, 848–917.

Barrat, J. A., S. Fourcade, B. M. Jahn, J. L. Cheminée, and R. Capdevila (1998), Isotope (Sr, Nd, Pb, O) and trace-element geochemistry of volcanics from the Erta'Ale range (Ethiopia), *J. Volcanol. Geotherm. Res.*, *80*, 85–100.

Beermann, O., R. E. Botcharnikov, F. Holtz, O. Diedrich, and M. Nowak (2012), Temperature dependence of sulfide and sulfate solubility in olivine-saturated basaltic magmas, *Geochim. Cosmochim. Acta*, *75*, 7612–7631.

Behrens, H., and J. Stelling (2011), Diffusion and redox reactions of sulfur in silicate melts, in *Sulfur in Magmas and Melts: Its Importance for Natural and Technical Processes*, edited by H. Behrens and J. D. Webster, pp. 79–111, The Mineral. Soc. of Am., Chantilly, Va.

Benhamou, G., P. Allard, J. C. Sabroux, G. Vitter, D. Dajlevic, and A. Creusot, (1988), Oxygen fugacity of gases and rocks from Momotombo volcano, Nicaragua: Application to volcanological monitoring, *J. Geophys. Res.*, *93*, 14872–14880.

Bizouard, H., F. Barberi, and J. Varet (1980), Mineralogy and petrology of Erta Ale and Boina volcanic series, Afar Rift, Ethiopia, *J. Petrol.*, *21*, 401–436.

Bluth, G. J. S., C. C. Schnetzler, A. J. Krueger, and L. S. Walter (1993), The contribution of explosive volcanism to global atmospheric sulfur dioxide concentrations, *Nature*, *366*, 327–329.

Bosworth, W., P. Huchon, and K. McClay (2005), The Red Sea and Gulf of Aden basins, *J. Afr. Earth Sci.*, *43*, 334–378.

Bouche, E., S. Vergniolle, T. Staudacher, A. Nercessian, J.-C. Delmont, M. Frogneux, F. Cartault, and A. Le Pichon (2010), The role of large bubbles detected from acoustic measurements on the dynamics of Erta 'Ale lava lake (Ethiopia), *Earth Planet. Sci. Lett.*, *295*, 37–48.

Brown, L., J. Klein, R. Middleton, I. S. Sacks, and F. Tera (1982), ^{10}Be in island arc volcanoes and implications for subduction, *Nature*, *299*, 718–720.

Burgisser, A., and B. Scaillet (2007), Redox evolution of a degassing magma rising to the surface, *Nature*, *445*, 194–197.

Burton, M. R., C. Oppenheimer, L. A. Horrocks, and P.W. Francis (2000), Remote sensing of CO_2 and H_2O emission rates from Masaya volcano, Nicaragua, *Geology, 28*, 915–918.

Carr, M. J., and W. I. Rose (1987), Centam—A database of Central-American volcanic-rocks, *J. Volcanol. Geotherm. Res.*, *33*, 239–240.

Carr, M. J., M. D. Feigenson, and E. A. Bennett (1990), Incompatible element and isotopic evidence for tectonic control of source mixing and melt extraction along the Central-American Arc, *Contrib. Mineral. Petrol.*, *105*, 369–380.

Carroll, M. R., and J. D. Webster (1994), Solubilities of sulfur, noble-gases, nitrogen, chlorine, and fluorine in magmas, in *Volatiles in Magmas*, edited by M. R. Carroll and J. R. Holloway, pp. 231–279, *Mineral. Soc. Am.*, Washington.

Chaussidon, M., F. Albarède, and S. M. F. Sheppard (1987), Sulfur isotope heterogeneity in the mantle from ion microprobe measurements of sulfide inclusions in diamonds, *Nature*, *330*, 242–244.

Cottrell, E., and K. A. Kelley (2011), The oxidation state of Fe in MORB glasses and the oxygen fugacity of the upper mantle, *Earth Planet. Sci. Lett.*, *305*, 270–282.

Cottrell, E., K. A. Kelley, A. Lanzirotti, and R. A. Fischer (2009), High-precision determination of iron oxidation state in silicate glasses using XANES, *Chem. Geol.*, *268*, 167–179.

Darrah, T. H., D. Tedesco, F. Tassi, O. Vaselli, E. Cuoco, and R. J. Poreda (2013), Gas chemistry of the Dallol region of the Danakil depression in the Afar region of the northernmost East African Rift, *Chem. Geol.*, *339*, 16–29.

de Hoog, J. C. M., B. E. Taylor, and M. J. van Bergen (2001), Sulfur isotope systematics of basaltic lavas from Indonesia: Implications for the sulfur cycle in subduction zones, *Earth Planet. Sci. Lett.*, *189*, 237–252.

Delmelle, P., A. Bernard, M. Kusakabe, T. P. Fischer, and B. Takano (2000), Geochemistry of the magmatic-hydrothermal system of Kawah Ijen volcano, East Java, Indonesia, *J. Volcanol. Geotherm. Res.*, *97*, 31–53.

DeMets, C. (2001), A new estimate for present-day Cocos-Caribbean plate motion: Implications for slip along the Central American volcanic arc, Geophys, *Res. Lett.*, *28*, 4043–4046, doi:10.1029/2001GL013518.

de Moor, J. M., T. P. Fischer, D. R. Hilton, E. Hauri, L. A. Jaffe, and J. T. Camacho (2005), Degassing at Anatahan volcano during the May 2003 eruption: Implications from petrology, ash leachates, and SO_2 emissions, *J. Volcanol. Geotherm. Res.*, *146*, 117–138.

de Moor, J. M., T. P. Fischer, Z. D. Sharp, E. H. Hauri, D. R. Hilton, and V. Atudorei (2010), Sulfur isotope fractionation during the May 2003 eruption of Anatahan volcano, Mariana Islands: Implications for sulfur sources and plume processes, *Geochim. Cosmochim. Acta*,*74* , 5382–5397.

Elkins, L. J., T. P. Fischer, D. R. Hilton, Z. D. Sharp, S. McKnight, and J. Walker (2006), Tracing nitrogen in volcanic and geothermal volatiles from the Nicaraguan volcanic front, *Geochim. Cosmochim. Acta*, *70*, 5215–5235.

Evans, K. A. (2012), The redox budget of subduction zones, *Earth Sci. Rev.*, *113*, 11–32.

Field, L., T. Barnie, J. Blundy, R. A. Brooker, D. Keir, E. Lewi, and K. Saunders (2012), Integrated field, satellite and petrological observations of the November 2010 eruption of Erta Ale, *Bull. Volcanol.*, *74*, 2251–2271.

Freda, C., D. R. Baker, and P. Scarlato (2005), Sulfur diffusion in basaltic melts, *Geochim. Cosmochim. Acta*, *69*, 5061–5069.

Fry, B., S. R. Silva, C. Kendall, and R. K. Anderson (2002), Oxygen isotope corrections for online δ34S analysis, *Rapid Commun. Mass Spectrom.*, *16*, 854–858.

Frost, B. R. (1991), Introduction to oxygen fugacity and its petrologic importance, *in Oxide Minerals : Petrologic and Magnetic Significance*, edited by D. H. Lindsley, pp. 1-9, Mineralogical Society of America.

Gaillard, F., and B. Scaillet (2009), The sulfur content of volcanic gases on Mars, *Earth Planet. Sci. Lett.*, *279*, 34–43, doi:10.1016/j.epsl.2008.12.028.

Gaillard, F., B. Scaillet, and N. T. Arndt (2011), Atmospheric oxygenation caused by a change in volcanic degassing pressure, *Nature*, *478*, 229–232.

Galle, B., C. Oppenheimer, A. Geyer, A. J. S. McGonigle, M. Edmonds, and L. Horrocks (2002), A miniaturized ultraviolet spectrometer for remote sensing of SO_2 fluxes: A new tool for volcano surveillance, *J. Volcanol. Geotherm. Res.*, *119*, 241–254.

Gerlach, T. M. (1980), Investigation of volcanic gas-analyses and magma outgassing from Erta-Ale lava lake, Afar, Ethiopia, *J. Volcanol. Geotherm. Res.*, *7*, 415–441.

Gerlach, T. M., H. R. Westrich, and R. B. Symonds (1996), Pre-eruptive vapor in magma of the climactic Mount Pinatubo eruption: Source of the giant stratospheric sulfur dioxide cloud, in *Fire and Mud: Eruptions and Lahars of Mount Pinatubo, Phillipines*, edited by C. G. Newhall and R. S. Punongbayan, pp. 415–433, Univ. of Wash. Press, Seattle, Wash.

Gerlach, T. M. (1993), Oxygen buffering of Kilauea volcanic gases and the oxygen fugacity of Kilauea basalt, *Geochimica et Cosmochimica Acta*, *57*, 795–814.

Giggenbach, W. F. (1987), Redox processes governing the chemistry of fumarolic gas discharges from White Island, New Zealand, *Appl. Geochem.*, *2*, 143–161.

Giggenbach, W. F. (1996), Chemical composition of volcanic gas, in *IAVCEI-UNESCO: Monitoring and Mitigation of Volcanic Hazards*, edited by R. Tilling, pp. 221–256, Springer, Berlin.

Giggenbach, W. F., and R. L. Goguel (1989), *Methods for the Collection and Analysis of Geothermal and Volcanic Water and Gas Samples*, vol. *53*, Chem. Div., Dept. of Sci. and Ind. Res., Petone, New Zealand.

Giggenbach, W. F., and F. Le Guern (1976), The chemistry of magmatic gases from Erta'Ale, Ethiopia, *Geochim. Cosmochim. Acta*, *40*, 25–30.

Goff, F., J. Gardner, R. Vidale, and R. Charles (1985), Geochemistry and isotopes of fluids from Sulfur Springs, Valles Caldera, New-Mexico, *J. Volcanol. Geotherm. Res.*, *23*, 273–297.

Goff, F., C. J. Janik, H. Delgado, C. Werner, D. Counce, J. A. Stimac, C. Siebe, S. P. Love, S. N. Williams, T. Fischer, and L. Johnson (1998), Geochemical surveillance of magmatic volatiles at Popocatepetl volcano, Mexico, *Geolog. Soc. Amer. Bull.*, *110*, 695–710.

Graf, H. F., J. Feichter, and B. Langmann (1997), Volcanic sulfur emissions: Estimates of source strength and its

contribution to the global sulfate distribution, *J. Geophys. Res.*, *102*, 10,727–10,738.

Gurenko, A. A., et al. (2001), Magma ascent and contamination beneath one intraplate volcano: Evidence from S and O isotopes in glass inclusions and their host clinopyroxenes from Miocene basaltic hyaloclastites southwest of Gran Canaria (Canary Islands), *Geochim. Cosmochim. Acta*, *65*, 4359–4374.

Halevy, I., M. T. Zuber, and D. P. Schrag (2007), A sulfur dioxide climate feedback on early Mars, *Science*, *318*, 1903–1907.

Hammond, J. O. S., J.-M. Kendall, G. W. Stuart, D. Keir, C. Ebinger, A. Ayele, and M. Belachew (2011), The nature of the crust beneath the Afar triple junction: Evidence from receiver functions, *Geochem. Geophys. Geosyst.*, *12*, Q12004, doi:10.1029/2011GC003738.

Haughton, D. R., P. L. Roeder, and B. J. Skinner (1974), Solubility of sulfur in mafic magmas, *Econ. Geol.*, *69*, 451–467.

Hilton, D. R., T. P. Fischer, and B. Marty (2002), Noble gases and volatile recycling at subduction zones, in *Noble Gases in Geochemistry and Cosmochemistry*, edited by D. Porcelli, C. J. Ballentine, and R. Wieler, *Mineral. Soc. Am.*, Washington, D. C., pp. 319–370.

Holland, T., and R. Powell (1991), A Compensated-Redlich-Kwong (Cork) equation for volumes and fugacities of CO_2 and H_2O in the Range 1-Bar to 50-Kbar and 100–1600-degrees C, *Contrib. Mineral. Petrol.*, *109*, 265–273.

Holloway, J. R., and J. G. Blank (1994), Application of experimental results to C-O-H species in natural melts, in *Volatiles in Magmas*, edited by M. R. Carroll and J. R. Holloway, pp. 187–230, Mineral. Soc. of Am., Fredericksburg, Va.

Holser, W. T., et al. (1988), Biogeochemical cycles of carbon and sulfur, in *Chemical Cycles in the Evolution of the Earth*, edited by B. Gregor, et al., pp. 105–174, John Wiley, New York.

Horrocks, L. A. (2001), *Infrared Spectroscopy of Volcanic Gases at Masaya, Nicaragua*, The Open Univ., Milton Keynes.

Johnson, S. S., M. A. Mischna, T. L. Grove, and M. T. Zuber (2008), Sulfur-induced greenhouse warming on early Mars, *J. Geophys. Res.*, *113*, E08005, doi:10.1029/2007JE002962.

Jugo, P. J., R. W. Luth, and J. P. Richards (2005), Experimental data on the speciation of sulfur as a function of oxygen fugacity in basaltic melts, *Geochim. Cosmochim. Acta*, *69*, 497–503.

Jugo, P. J., M. Wilke, and R. E. Botcharnikov (2010), Sulfur K-edge XANES analysis of natural and synthetic basaltic glasses: Implications for S speciation and S content as function of oxygen fugacity, *Geochim. Cosmochim. Acta*, *74*, 5926–5938.

Kazahaya, K., et al. (1994), Excessive degassing of Izu-Oshima volcano—Magma convection in a conduit, *Bull. Volcanol.*, *56*, 207–216.

Kelley, K. A., and E. Cottrell (2009), Water and the oxidation state of subduction zone magmas, *Science*, *325*, 605–607.

Kelley, K. A., and E. Cottrell (2012), The influence of magmatic differentiation on the oxidation state of Fe in a basaltic arc magma, *Earth Planet. Sci. Lett.*, *329*, 109–121.

Kiba, T., T. Takagi, Y. Yoshimura, and I. Kishi (1955), Tin(II)-strong phosphoric acid. A new reagent for the determination of sulfate by reduction to hydrogen sulfide, *Bull. Chem. Soc. Jpn.*, *28*, 645–649.

Klimm, K., S. C. Kohn, and R. E. Botcharnikov (2012), The dissolution mechanism of sulphur in hydrous silicate melts. II: Solubility and speciation of sulphur in hydrous silicate melts as a function of fO_2, *Chem. Geol.*, *322*, 250–267.

Kress, V. C., and I. S. E. Carmichael (1991), The compressibility of silicate liquids containing Fe_2O_3 and the effect of composition, temperature, oxygen fugacity and pressure on their redox states, *Contrib. Mineral. Petrol.*, *108*, 82–92.

Kurtz, A. C., L. R. Kump, M. A. Arthur, J. C. Zachos, and A. Paytan (2003), Early Cenozoic decoupling of the global carbon and sulfur cycles, *Paleoceanography*, *18*(4), 1090, doi:10.1029/2003PA000908.

Le Guern, F., J. Carbonnelle, and H. Tazieff (1979), Erta Ale lava lake: Heat and gas transfer to the atmosphere, *J. Volcanol. Geotherm. Res.*, *6*, 27–48.

Lee, C.-T. A., P. Luffi, E. J. Chin, R. Bouchet, R. Dasgupta, D. M. Morton, V. L. Roux, Q.-Z. Yin, and D. Jin (2012), Copper systematics in Arc Magmas and implications for Crust-Mantle Differentiation, *Science*, *336*, 64–68.

Lesne, P., S. C. Kohn, J. Blundy, F. Witham, R. E. Botcharnikov, and H. Behrens (2011), Experimental simulation of closed-system degassing in the system basalt-H_2O-CO_2-S-Cl, *J. Petrol.*, *52*, 1737–1762.

Li, C. S., and E. M. Ripley (2009), Sulfur contents at sulfide-liquid or anhydrite saturation in silicate melts: Empirical equations and example applications, *Econ. Geol.*, *104*, 405–412.

Liotta, M., A. Rizzo, A. Paonita, A. Caracausi, and M. Martelli (2012), Sulfur isotopic compositions of fumarolic and plume gases at Mount Etna (Italy) and inferences on their magmatic source, *Geochem. Geophys. Geosyst.*, *13*, Q05015, doi:10.1029/2012GC004118.

Liu, Y. N., N.-T. Samaha, and D. R. Baker (2007), Sulfur concentration at sulfide saturation (SCSS) in magmatic silicate melts, *Geochim. Cosmochim. Acta*, *71*, 1783–1799.

MacKenzie, L., G. A. Abers, K. M. Fischer, E. M. Syracuse, J. M. Protti, V. Gonzalez, and W. Strauch (2008), Crustal structure along the southern Central American volcanic front, *Geochem. Geophys. Geosyst.*, *9*, Q08S09, doi:10.1029/2008GC001991.

Mandeville, C., N. Shimizu, K. A. Kelley, and N. Metrich (2010), Sulfur isotope variation in arc basalts revealed by secondary ionization mass spectrometry: Measurements of melt inclusions, *Geochim. Cosmochim. Acta*, *74*, A663–A663.

Mandeville, C. W., A. Sasaki, G. Saito, K. Faure, R. King, and E. Hauri (1998), Open-system degassing of sulfur from Krakatau 1883 magma, *Earth Planet. Sci. Lett.*, *160*, 709–722.

Mandeville, C. W., J. D. Webster, C. Tappen, B. E. Taylor, A. Timbal, A. Sasaki, E. Hauri, and C. R. Bacon (2009), Stable isotope and petrologic evidence for open-system degassing during the climactic and pre-climactic eruptions of Mt. Mazama, Crater Lake, Oregon, *Geochim. Cosmochim. Acta*, *73*, 2978–3012.

Marini, L., R. Moretti, and M. Accornero (2011), Sulfur isotopes in magmatic-hydrothermal systems, melts, and magmas, in *Sulfur in Magmas and Melts: Its Importance for Natural and Technical Processes*, edited by H. Behrens and J. D. Webster, pp. 423–492, The Mineral. Soc. of Am., Chantilly, Va.

Martin, E., and O. Sigmarsson (2007), Low-pressure differentiation of tholeiitic lavas as recorded in segregation veins from Reykjanes (Iceland), Lanzarote (Canary Islands) and Masaya (Nicaragua), *Contrib. Mineral. Petrol.*, *154*, 559–573.

Martin, R. S., et al. (2010), A total volatile inventory for Masaya Volcano, Nicaragua, *J. Geophys. Res.*, *115*, B09215, doi:10.1029/2010JB007480.

Martin, R. S., G. M. Sawyer, J. A. Day, J. S. LeBlond, E. Ilyinskaya, and C. Oppenheimer, (2012), High-resolution size distributions and emission fluxes of trace elements from Masaya volcano, Nicaragua, *Journal of Geophysical Research-Solid Earth*, 117.

Marty, B., R. Pik, and Y. Gezahegn (1996), Helium isotopic variations in Ethiopian plume lavas: Nature of magmatic sources and limit on lower mantle contribution, *Earth Planet. Sci. Lett.*, *144*, 223–237.

Mather, T. A., J. R. McCabe, V. K. Rai, M. H. Thiemens, D. M. Pyle, T. H. E. Heaton, H. J. Sloane, and G. R. Fern (2006a), Oxygen and sulfur isotopic composition of volcanic sulfate aerosol at the point of emission, *J. Geophys. Res.*, *111*, D18205, doi:10.1029/2005JD006584.

Mather, T. A., D. M. Pyle, V. I. Tsanev, A. J. S. McGonigle, C. Oppenheimer, and A. G. Allen (2006b), A reassessment of current volcanic emissions from the Central American arc with specific examples from Nicaragua, *J. Volcanol. Geotherm. Res.*, *149*, 297–311.

Mather, T. A., D. M. Pyle, and T. H. E. Heaton, (2008), Investigation of the use of filter packs to measure the sulphur isotopic composition of volcanic sulphur dioxide and the sulphur and oxygen isotopic composition of volcanic sulphate aerosol, *Atmos. Environ.*, *42*, 4611–4618.

Menyailov, I. A., L. P. Nikitina, V. N. Shapar, and V. P. Pilipenko (1986), Temperature increase and chemical change of fumarolic gases at Momotombo volcano, Nicaragua, in 1982–1985: Are these indicators of a possible eruption?, *J. Geophys. Res.*, *91*, 12,199–112,214.

Métaxian, J. P., P. Lesage, and J. Dorel (1997), Permanent tremor of Masaya Volcano, Nicaragua: Wave field analysis and source location, *J. Geophys. Res.*, *102*, 22,529–22,545.

Metrich, N., A. J. Berry, H. St. C. O'Neill, and J. Susini (2009), The oxidation state of sulfur in synthetic and natural glasses determined by X-ray absorption spectroscopy, *Geochim. Cosmochim. Acta*, *73*, 2382–2399.

Metrich, N., A. Bertagnini, and A. Di Muro (2010), Conditions of magma storage, degassing and ascent at Stromboli: New insights into the volcano plumbing system with inferences on the eruptive dynamics, *J. Petrol.*, *51*, 603–626.

Mitchell, E. C., T. P. Fischer, D. R. Hilton, E. H. Hauri, A. M. Shaw, J. M. de Moor, Z. D. Sharp, and K. Kazahaya (2010), Nitrogen sources and recycling at subduction zones: Insights from the Izu-Bonin-Mariana arc, *Geochem. Geophys. Geosyst.*, *11*, Q02X11, doi:10.1029/2009GC002783.

Miyoshi, T., H. Sakai, and H. Chiba (1984), Experimental study of sulfur isotope fractionation factors between sulphate and sulfide in high temperature melts, *Geochem. J.*, *18*, 75–84.

Moune, S., F. Holtz, and R. E. Botcharnikov (2009), Sulphur solubility in andesitic to basaltic melts: Implications for Hekla volcano, *Contrib. Mineral. Petrol.*, *157*, 691–707.

Nadeau, O., A. E. Williams-Jones, and J. Stix (2010), Sulphide magma as a source of metals in arc-related magmatic hydrothermal ore fluids, *Nat. Geosci.*, *3*, 501–505.

Nadeau, P. A., and G. Williams-Jones (2009), Apparent downwind depletion of volcanic SO_2 flux-lessons from Masaya Volcano, Nicaragua, *Bull. Volcanol.*, *71*, 389–400.

Nilsson, K., and C. L. Peach (1993), Sulfur speciation, oxidation state, and sulfur concentration in backarc magmas, *Geochim. Cosmochim. Acta*, *57*, 3807–3813.

O'Neill, H. S. C., and J. A. Mavrogenes (2002), The sulfide capacity and the sulfur content at sulfide saturation of silicate melts at 1400 degrees C and 1 bar, *J. Petrol.*, *43*, 1049–1087.

Oppenheimer, C., and P. Francis (1997), Remote sensing of heat, lava and fumarole emissions from Erta'Ale volcano, Ethiopia, *Int. J. Remote Sens.*, *18*, 1661–1692.

Ohba, T., K. Nogami, J. I. Hirabayashi, and T. Mori. (2008), Isotopic fractionation of SO_2 and H_2S gases during the absorption by KOH solution, with the application to volcanic gas monitoring at Miyakejima Island, Japan, *Geochemical Journal*, *42*, 119–131.

Oppenheimer, C., A. J. S. McGonigle, P. Allard, M. J. Wooster, and V. Tsanev (2004), Sulfur, heat, and magma budget of Erta 'Ale lava lake, Ethiopia, *Geology*, *32*, 509–512.

Pallister, J. S., F. A. Trusdell, I. K. Brownfield, D. F. Siems, J. R. Budahn, and S. F. Sutley (2005), The 2003 phreatomagmatic eruption of Anatahan volcano? Textural and petrological characteristics of eruptive products from an emergent volcano, *J. Volcanol. Geotherm. Res.*, *146*, 208–225.

Palma, J. L., S. Blake, and E. S. Calder (2011), Constraints on the rates of degassing and convection in basaltic open-vent volcanoes, *Geochem. Geophys. Geosyst.*, *12*, Q11006, doi:10.1029/2011GC003715.

Pik, R., B. Marty, and D. R. Hilton (2006), How many mantle plumes in Africa? The geochemical point of view, *Chem. Geol.*, *226*, 100–114.

Platt, U. (1994), Differential optical absorbption spectroscopy (DOAS), in *Air Monitoring by Spectroscopic Techniques*, edited by M. W. Sigrist, pp. 27–84, John Wiley, New York.

Putirka, K. D. (2008), Thermometers and barometers for volcanic systems, in *Minerals, Inclusions and Volcanic Processes*, edited by K. D. Putirka and F. J. Tepley, pp. 61–120, The Mineral. Soc. of Am., Chantilly, Va.

Richet, P., Y. Bottinga, and M. Janoy (1977), A review of hydrogen, carbon, nitrogen, oxygen, sulfur, and chlorine stable isotope fractionation among gaseous molecules, *Annu. Rev. Earth Planet. Sci.*, *5*, 65–110.

Ritsema, J., H. J. van Heijst, and J. H. Woodhouse (1999), Complex shear wave velocity structure imaged beneath Africa and Iceland, *Science*, *286*, 1925–1928.

Robie, R. A., and B. S. Hemingway (1995), Thermodynamic properties of minerals and related substances at 298.15 K and 1 Bar (10^5 Pascals) pressure and at higher temperatures, *U.S. Geol. Surv. Bull.*, *2131*, 461.

Robinson, B. W. (1995), Sulfur isotope standards, in Reference and Intercomparison Materials for Stable Isotopes of Llight Elements, Proceedings of a Consultants Meeting, Vienna, 1–3 Dec, IAEA-TECDOC-825, Int. At. Energy Agency, Vienna.

Rowe, G. L. (1994), Oxygen, hydrogen, and sulfur isotope systematics of the crater lake system of Poas volcano, Costa-Rica, *Geochem. J.*, *28*, 263–287.

Rye, R. O. (2005), A review of the stable-isotope geochemistry of sulfate minerals in selected igneous environments and related hydrothermal systems, *Chem. Geol.*, *215*, 5–36.

Rymer, H., B. van Wyk de Vries, J. Stix, and G. Williams-Jones (1998), Pit crater structure and processes governing persistent activity at Masaya Volcano, Nicaragua, *Bull. Volcanol.*, *59*, 345–355.

Sadofsky, S. J., M. Portnyagin, K. Hoernle, and P. van den Bogaard (2008), Subduction cycling of volatiles and trace elements through the Central American volcanic arc: Evidence from melt inclusions, *Contrib. Mineral. Petrol.*, *155*, 433–456.

Sakai, H., T. J. Casadevall, and J. G. Moore (1982), Chemistry and isotope ratios of sulfur in basalts and volcanic gases at Kilauea Volcano, Hawaii, *Geochim. Cosmochim. Acta*, *46,* 729–738.

Sakai, H., D. J. Des Marais, A. Ueda, and J. G. Moore (1984), Concentrations and isotope ratios of carbon, nitrogen, and sulfur in ocean-floor basalts, *Geochim. Cosmochim. Acta*, *48*, 2433–2441.

Sasaki, A., Y. Arikawa, and R. E. Folinsbee (1979), Kiba reagent method of sulfur extraction applied to isotopic work, *Bull. Geol. Surv. Jpn.*, *30*, 241–245.

Sawyer, G. M., C. Oppenheimer, V. I. Tsanev, and G. Yirgu (2008), Magmatic degassing at Erta 'Ale volcano, Ethiopia, *J. Volcanol. Geotherm. Res.*, *178*, 837–846.

Schauble, E. A. (2004), Applying stable isotope fractionation theory to new systems, in *Geochemistry of Non-Traditional Stable Isotopes*, edited by C. M. Johnson, B. L. Beard, and F. Albarede, pp. 65–111, The Mineral. Soc. of Am., Chantilly, Va.

Settle, M. (1979), Formation and deposition of volcanic sulfate aerosols on Mars, *J. Geophys. Res.*, *84*, 8343–8354.

Shinohara, H. (2008), Excess degassing from volcanoes and its role on eruptive and extrusive activity, *Rev. Geophys.*, *46*, RG4005, doi:10.1029/2007RG000244.

Shishkina, T. A., R. E. Botcharnikov, F. Holtz, R. R. Almeev, and M. V. Portnyagin (2010), Solubility of H_2O- and CO_2-bearing fluids in tholeiitic basalts at pressures up to 500 MPa, *Chem. Geol.*, *277*, 115–125.

Sigurdsson, H. (1990), *Assessment of the atmospheric impact of volcanic eruptions, in Global Catastrophes in Earth History*, edited by V. I. Sharpton and P. D. Ward, pp. 99–110, Geol. Soc. of Am. Spec. Pap., Seattle, Washington.

Sisson, T. W. (2003), Native gold in a Hawaiian alkalic magma, *Econ. Geol. Bull. Soc. Econ. Geol.*, *98*, 643–648.

Sparks, R. S. J. (2003), Dynamics of magma degassing, in *Volcanic Degassing*, edited by C. Oppenheimer, D. M. Pyle, and J. Barclay, pp. 5–22, The Geol. Soc., London.

Sparks, R. S. J., J. Barclay, C. Jaupart, H. M. Mader and J. C. Phillips (1994), Physical aspects of magmatic degassing.1. Experimental and theoretical constraints on vesiculation, *Volatiles Magmas*, *30*, 413–445.

Spilliaert, N., P. Allard, N. Métrich, and A. V. Sobolev (2006), Melt inclusion record of the conditions of ascent, degassing, and extrusion of volatile-rich alkali basalt during the powerful 2002 flank eruption of Mount Etna (Italy), *J. Geophys. Res.*, *111*, B04203, doi:10.1029/2005JB003934.

Stix, J. (2007), Stability and instability of quiescently active volcanoes: The case of Masaya, Nicaragua, *Geology*, *35*, 535–538.

Stoiber, R. E., L. L. Malinconico, and S. N. Williams (1983), Use of the correlation spectrometer at volcanoes, in *Forecasting Volcanic Events*, edited by H. S. Tazieff, pp. 424–444, Elsevier, New York.

Stoiber, R. E., S. N. Williams, and B. J. Huebert (1986), Sulfur and halogen gases at Masaya Caldera Complex, Nicaragua—Total flux and variations with time, *J. Geophys. Res.*, *91*, 2215–2231.

Taran, Y., J. C. Gavilanes, and A. Cortés (2002), Chemical and isotopic composition of fumarolic gases and the SO_2 flux from Volcan de Colima, Mexico, between the 1994 and 1998 eruptions, *J. Volcanol. Geotherm. Res.*, *117*, 105–119.

Taran, Y. A., J. W. Hedenquist, M. A. Korzhinsky, S. I. Tkachenko, and K. I. Shmulovich (1995), Geochemistry of magmatic gases from Kudryavy Volcano, Iturup, Kuril Islands, *Geochim. Cosmochim. Acta*, *59*, 1749–1761.

Ueda, A., and H. Sakai (1984), Sulfur isotope study of quaternary volcanic rocks from the Japanese Islands Arc, *Geochim. Cosmochim. Acta*, *48*, 1837–1848.

Venzke, E., et al. (2002), *Global Volcanism*, 1968 to the present, Global Volcanism Prog. Digital Inf. Ser. GVP-4, Smithsonian Inst., Washington, D. C. [Available at http://www.volcano.si.edu/reports/.]

Walker, J. A. (1989), Caribbean arc tholeiites, *J. Geophys. Res.*, *94*, 10,539–10,548.

Walker, J. A., S. N. Williams, R. I. Kalamarides, and M. D. Feigenson (1993), Shallow open-system evolution of basaltic magma beneath a subduction zone volcano—The Masaya Caldera Complex, Nicaragua, *J. Volcanol. Geotherm. Res.*, *56*, 379–400.

Wallace, P., and I. S. E. Carmichael (1992), Sulfur in basaltic magmas, *Geochim. Cosmochim. Acta*, *56*, 1863–1874.

Wallace, P. J., and I. S. E. Carmichael (1994), S-speciation in submarine basaltic glasses as determined by measurements of Sk-alpha X-Ray wavelength shifts, *Am. Mineral.*, *79*, 161–167.

Wallace, P. J., and M. Edmonds (2011), The sulfur budget in magmas: Evidence from melt inclusions, submarine glasses, and volcanic gas emissions, in *Sulfur in Magmas and Melts: Its Importance for Natural and Technical Processes*, edited by H. Behrens and J. D. Webster, pp. 215–246, The Mineral. Soc. of Am., Chantilly, Va.

Wehrmann, H., K. Hoernle, M. Portnyagin, M. Wiedenbeck and K. Heydolph (2011), Volcanic CO2 output at the Central American subduction zone inferred from melt inclusions in olivine crystals from mafic tephras, *Geochem. Geophys. Geosyst.*, 12.

Webster, J. D., and R. E. Botcharnikov (2011), Distribution of sulfur between melt and fluid in S-O-H-C-Cl-bearing magmatic systems at shallow crustal pressures and temperatures, in *Sulfur in Magmas and Melts: Its Importance for Natural and Technical Processes*, edited by H. Behrens and J. D. Webster, pp. 247–283, The Mineral. Soc. of Am., Chantilly, Va.

Wilke, M., P. J. Jugo, K. Klimm, J. Susini, R. Botcharnikov, S. C. Kohn, and M. Janousch (2008), The origin of S^{4+} detected in silicate glasses by XANES, *Am. Mineral.*, *93*, 235–240.

Wilke, M., K. Klimm, and S. Kohn (2011), Spectroscopic studies on sulfur speciation in synthetic and natural glasses, in *Sulfur in Magmas and Melts: Its Importance for Natural and Technical Processes*, edited by H. Behrens and J. D. Webster, pp. 41–78, The Mineral. Soc. of Am., Chantilly, Va.

Williams, S. N. (1983), *Geology and eruptive mechanisms of Masaya Caldera Complex, Nicaragua*, PhD thesis, 169 pp., Dartmouth Coll., Hanover, N. H.

Williams-Jones, G., H. Rymer, and D. A Rothery (2003), Gravity changes and passive SO_2 degassing at the Masaya caldera complex, Nicaragua, *J. Volcanol. Geotherm. Res.*, *123*, 137–160.

Witter J. B., V. C. Kress, and C. G. Newhall (2005), Volcan Popocatepetl, Mexico. Petrology, magma mixing, and immediate sources of volatiles for the 1994 - Present eruption, *J. Petrol.*, *46*, 2337–2366.

Yasuda A., , Nakada S., and Fujii T., (2001), Sulfur abundance and redox state of melt inclusions from Miyake-jima 2000 eruption products, *Bull. Volcanol. Soc., Japan*., *46*, 165–173.

Zelenski, M. E., T. P. Fischer, J. M. de Moor, B. Marty, L. Zimmermann, D. Ayalew, A. N. Nekrasov, and V. K. Karandashev (2013), Trace elements in the gas emissions from the Erta-Ale volcano, Afar, Ethiopia, *Chem. Geol.*, 357, 95–116.

Zhang, Y. X. (2010), Diffusion in minerals and melts theoretical background, in Diffusion in Minerals and Melts, edited by Y. X. Zhang, D. J. Cherniak, *Mineral. Soc. Am.*, Chantilly, VA, pp. 5–57.